Title
Neuronal Circuitry of the Local Edge Detector Retinal Ganglion Cell

Author
Russell, Thomas Lee

Publication Date
2010

Peer reviewed|Thesis/dissertation

Neuronal Circuitry of the Local Edge Detector Retinal Ganglion Cell

by

Thomas Lee Russell

A dissertation submitted in partial satisfaction of the

requirements for the degree of

Doctor of Philosophy

in

Molecular and Cell Biology

in the

Graduate Division

of the

University of California, Berkeley

Committee in charge:

Professor Frank Werblin, Chair
Professor Lu Chen
Professor Laurent Coscoy
Professor Michael Silver

Fall 2010

Neuronal Circuitry of the Local Edge Detector Retinal Ganglion Cell

By Thomas Lee Russell

Abstract

Neuronal Circuitry of the Local Edge Detector Retinal Ganglion Cell

by

Thomas Lee Russell

Doctor of Philosophy in Molecular and Cell Biology

University of California, Berkeley

Professor Frank Werblin, Chair

Detection of visual borders is an essential function for transforming the visual scene into perceivable boundaries. Avian predators, for example, are able to recognize complex textured borders of conspicuous prey. It has been suggested that the process of border perception begins as early as in the retina through a class of ganglion cell, the local edge detector (LED), which responds selectively to luminance edges. But what neuronal circuitry is used to accomplish this, and can this circuitry also be used to detect complex textured borders? Here we use patch-clamp electrophysiology to show that selectivity to luminance edges in the LED is accomplished by surround-originated feedback inhibition that suppresses excitation via GABAa and GABAc receptors. Furthermore, we find that excitatory circuitry has several characteristics that facilitate independent responses of individual bipolar cells to features as small as one-eighth the size of the LED's receptive field. This enables the LED to respond to areas of texture even if they contain no net luminance change. We observed that feedback inhibition is similarly activated by small features, which in turn causes excitation not only to respond selectively to luminance edges, but also to boundaries of luminance-neutral texture in synthetic and natural scenes, as well as a noise-suppression function suggested by modeling. We also characterized direct feedforward inhibition to the LED, and found it to be cospatial with excitation, glycinergic, and sensitive to small features as well. These characteristics enable the suppression of spikes during rapid luminance shifts, encoding an "edge in time". Our results suggest mechanisms by which three kinds of edges can be encoded by the retina and transmitted through a specialized channel to higher visual areas in the brain.

ACKNOWLEDGEMENT

I would like to thank Ken Greenberg for providing the natural scene videos, and Sandra Siegert for her helpful comments. This work was supported by NIH grant #EY015512.

TABLE OF CONTENTS

FIGURES

INTRODUCTION

Edges in Sensory Systems

Sharp differences in qualitative content between neighboring locations in the visual scene often correspond to the physical boundaries of objects in space due to these objects having differing luminance, hue, and texture properties. It is therefore advantageous for organisms to be able to perceive these types of transitions as a prerequisite to the recognition of objects. This perception has been shown to be behaviorally relevant to survival: Conspicuous borders of texture make prey discernable to predators [1], and the various camouflaging methods evolved by prey species seem to function by blurring these borders [2]. It has also been shown that homing pigeons can navigate by following luminance edges that are present in the landscape and visible from the air [3, 4]. Yet the process of edge detection is a broadly applicable concept, not limited exclusively to vertebrate vision. The selective response to rapid signal transitions has also been studied in audition [5], the paddlefish electrosensory system [6], and fly ommatidium [7].

Computational Methods of Edge Detection

The process by which a visual scene is transformed into a signal that delineates sharp luminance transitions is commonly referred to by the general term "edge detection". The usefulness of this process has long been of interest to theorists and engineers of machine vision [8-13] . This interest has inspired the development of several classes of edge detection algorithms for images [14-17] , plus a nearly innumerable amount of variations (for a thorough treatment, see [18]).

One of the most prevalent edge detection filters is the Sobel filter. This is a so-called "first derivative" detector, which approximates the change in luminance at any given point on the image by convolving two kernels against and image (I) as follows:

Equation 1.

$$G_x = \begin{bmatrix} +1 & 0 & -1 \\ +2 & 0 & -2 \\ +1 & 0 & -1 \end{bmatrix} * I$$

Equation 2.

$$G_y = \begin{bmatrix} +1 & +2 & +1 \\ 0 & 0 & 0 \\ -1 & -2 & -1 \end{bmatrix} * I$$

And further applying Equation 3:

$$G = \sqrt{{G_x}^2 + {G_y}^2}$$

This gives an orientation-independent first derivative of the image's luminance for all points. An image (Figure 1A) with the above Sobel filter applied is shown in Figure 1B, with a cutout of a select area (within the orange oval) and its signal intensity profile to demonstrate the first-derivative nature of this edge detecting algorithm.

One problem with Sobel filters is that since they merely delineate locations of high luminance change, the ability to locate the edge precisely can be confounded if high luminance change exists anywhere near the edge, particularly perpendicular to it. Marr points out that the logical location of any edge should be where the first derivative peaks – the zero-crossing of luminance's second derivative. This led to the creation of a second class of edge detector that utilizes a difference-of-Gaussian function in which two Gaussian functions of approximate but unequal sigma values are subtracted. The result of this difference is a Laplacian function (Figure

1C), which is optimal for computing two-dimensional second derivatives in an orientation-independent manner, due to its localized center-surround antagonism. Such a derivation is generally obtained by convolving an approximated Laplacian kernel with an image (*I*): Equation 4.

$$L = \begin{bmatrix} 0 & -1 & 0 \\ -1 & 4 & -1 \\ 0 & -1 & 0 \end{bmatrix} * I$$

This operation was performed on Figure 1A to get Figure 1D. A cutout and intensity profile in Figure 1D demonstrates how this algorithm delineates zero crossings in edges.

Although edge-detection algorithms were not developed with biological vision in mind *per se*, we discuss later what similarities and differences exist between these algorithms and retinal circuit components, and how their functions correlate.

Retinal Circuitry: Building Blocks for Transforming the Visual Scene

The vertebrate retina contains two layers of synapses (outer plexiform layer (OPL) and inner plexiform layer (IPL), Figure 2). At the first stage of processing, cones respond to light striking them by modulating their glutamate release; luminance decrements elicit increases in glutamate, increments elicit decreases. Glutamate, in turn, drives bipolar cells and horizontal cells. Horizontal cells reside in the receptive field surround and modulate glutamate release at the cone-bipolar cell synapse in an antagonistic manner. For example, light decrements in the surround tend to decrease glutamate release, whereas light increments tend to increase glutamate release; the exact opposite of the response in the center [19-21]. This is accomplished by shifting the calcium current activation range in cone terminals by either a pH-mediated or hemichannel-mediated emphatic mechanism [22, 23]. This is the mechanism by which the first layer of center-surround antagonism is formed in the retina.

Bipolar cells encode increments and decrements of light (ON and OFF) [24], which is accomplished either by sign-preserving ionotropic glutamate receptors [25] or sign-inverting metabotropic glutamate receptors [26] on the dendrites of OFF and ON bipolar cells, respectively. Bipolar cells, in turn, secrete glutamate in the inner plexiform layer and drive ganglion cells and inhibitory interneurons called amacrine cells. Amacrine cells secrete either GABA or glycine [27, 28] and act at bipolar cell terminals to suppress their release (feedback inhibition) or inhibit ganglion cells directly (feedforward inhibition) [29, 30]. Ganglion cells send axons to higher visual centers such as the lateral geniculate nucleus or superior colliculus.

Although retinal circuits generally follow this layout, each one is a unique variation on the exact components and connections present. All circuits have cone photoreceptor to bipolar cell synapses, but some ganglion cells may only get excitatory input from either the ON or OFF system, or both. Bipolar cell diversity further adds to circuit variability; there are twelve distinct types of bipolar cells classified by morphology and depth of stratification into the inner plexiform layer [31], although their post-synaptic targets are constrained to ganglion cells that have dendrites in corresponding strata [32].

A large source of functional variability in retinal circuitry is derived from the presence of inhibition. Excitatory inputs to ganglion cells show unique spatio-temporal responses to light squares, which is presumably shaped by amacrine-to-bipolar cell feedback inhibition [33, 34]. Similar variability in feedforward inhibition is also seen [33, 34]. Some of this diversity of response may be a consequence of the morphological diversity seen in the amacrine cell

population. There are approximately twenty-seven morphological types of amacrine cells in the mammalian retina, having various dendritic field sizes and stratification patterns [35, 36]. Of these, only two (the AII and Starburst [37, 38]) have clearly defined functions. Any one or combination of these amacrine cells could supply feedback or feedforward inhibition, resulting in a unique shaping the response properties of bipolar and ganglion cells. Amacrine-to-amacrine cell inhibition can also further increase the complexity of light responses [39], suggesting that the bulk of the processing capabilities in the retina originate from the connectivity of inhibition.

Finally, ganglion cell dendritic field size is a crucial component of circuitry. There are approximately twelve ganglion cell types with dendritic field sizes ranging from 150 to 750 μm in width [40]. This allows the collection of ganglion cells in the retina to represent features at a wide range of sizes and spatial frequencies [41]. In fact, the encoding of edges of various sizes is a requirement for Marr and Hildreth's theory of edge perception in the visual system [15].

All of these classes of circuit components, including the ganglion cells themselves, form the toolbox with which the retina shapes the visual scene into the visual stream that courses through the optic nerve.

Edge Representation in the Visual Pathway

Cognitive vision scientists have recently become interested in how edges are processed and perceived in humans [42-44], and it has been long known that neurons in the cortex respond to oriented edges [45, 46]. Yet there is still an incomplete body of literature regarding visual edges at the pre-cortical systems level, which leaves the following questions unanswered: Where in the visual pathway are edge-specific signals formed, what neuronal circuitry enables it, and what are the information processing capabilities of this circuitry?

We hypothesized that processes leading to edge perception could begin as early as in the retina, and aimed to begin answering these questions by considering a class of ganglion cell in the rabbit retina called the local edge detector (LED). This cell responds with sustained spiking to luminance edges [33, 34], and was suggested in a computational study [47] to be capable of performing a type of edge detection proposed by Marr and Hildreth [15]. The LED was first described by Levick [48], who characterized its response as sluggish, with a narrow receptive field center. He found that drifting gratings confined to the center elicited vigorous spiking, but this spiking was strongly suppressed when the drifting stimulus was expanded to include the surround, suggesting a non-canonical lateral inhibitory component. This experiment provided the inspiration for its name due to the ability to respond to edges (gratings) which were "local" (i.e. in the center only).

Later work by van Wyk et al. [49] showed that the dendrites of the LED in rabbits span approximately 100 to 200 μm (the smallest of any ganglion cell) and overlap heavily with each other, suggesting a cell body spacing of approximately 30 μm near the visual streak. This implies that the function of the LED is performed at high visual resolution. Morphology resembling the LED is also found in several mammalian species [47, 50, 51] including macaque fovea [52], further implying a generalized high-acuity function. The unique response properties, high spatial resolution, and apparent ubiquity among species suggest a crucial, information-rich role in mammalian vision.

In this study, we defined the details of the neural circuitry that lead to the edge encoding properties of the LED. We pharmacologically dissected the excitatory and inhibitory pathways in the receptive field, using spatial stimuli designed to separate the center from the surround, and separate the two primary retinal synapse layers. We show that excitation receives strong gamma-

aminobutyric acid (GABA)-based lateral feedback inhibition, and that subreceptive field spatial tuning in the center and surround circuitry underlie its response properties. We conclude that these components combine to form a circuit that is capable of encoding both luminance edges and complex textured edges.

RESULTS

Receptive Field of Excitation and Feedforward Inhibition are Cospatial

Van Wyk et al. [49] measured a very narrow receptive field, approximately cospatial with the dendritic field of the LED, using spiking in response to spots of increased size. We repeated this experiment with patch clamp to determine the circuitry underlying the narrow receptive field. For this experiment, we measured the average current over the duration of each flashed spot, and normalized them against the largest average current for each cell. Figures 3A and 3B show excitation and feedforward inhibition in response to increasing spot sizes of OFF (-100% luminance) and ON (+300% luminance) polarity. OFF responses peaked at 150 µm, with a normalized value of 0.96 ± 0.03, and ON responses peaked at 200 µm, with a normalized value of 0.48 ± 0.05. These dimensions were similar to the anatomic dendritic field size (Figure 3C, 151.5 ± 7.6 µm) and the results of studies by Van Wyk et al. [49]. Both ON and OFF responses diminished sharply beyond 200 µm. OFF excitation in particular, at 500 µm, reduced to a normalized value of 0.07 ± 0.03 and remained statistically unchanged for greater spot sizes. ON excitation followed a similar pattern, diminishing to 0.21 ± 0.03 at 500 µm and beyond.

ON feedforward inhibition exhibited a similar antagonistic pattern, peaking at 150 µm with a normalized value of 0.76 ± 0.08, and flattening out at 500 µm with a normalized value of 0.32 ± 0.08. Surprisingly, the response of OFF inhibition did not diminish with increasing spot diameter; the response increased for spot sizes up to 100 µm, and then remained at that level well beyond 200 µm. These results suggest that the surround antagonisms of the ON and OFF excitatory receptive fields, and the ON component of the inhibitory field, are formed presynaptically, and are not mediated through interactions between excitation and inhibition at the membrane of the LED. Furthermore, peaks in excitation at 150 µm provide a clear, spatial delineation between center and surround, a parameter that we used in later experiments.

ON and OFF Excitatory Inputs to the Local Edge Detector Are Rectified.

Figure 3E shows average excitatory currents recorded from an LED in response to a dark (-100% luminance) then light (+300% luminance) 200-µm diameter spot. The control showed robust responses at both ON and OFF phases, as expected. Application of APB eliminated the ON phase, suggesting that the ON response was derived from mGluR6-expressing ON bipolar cells. Furthermore, there was no apparent outward current during the ON phase in APB, as would be expected if OFF bipolar input were nonrectified. This indicates that the OFF system is rectified and does not provide tonic glutamate input to the LED that is reduced at ON illumination.

Figure 3D illustrates how this can occur. If OFF excitation were not rectified, an outward current would be generated during ON illumination. This would not normally be observed but would be revealed during mGluR6 blockage, owing to ON and OFF excitation no longer being mixed. Under this pharmacologic condition, we can infer that ON excitation is also rectified; Figure 3D indicates that nonrectified ON bipolar input would produce an *increase* in OFF excitation in the presence of APB. However, we never measured such an outward current at ON illumination or an increase in currents at OFF illumination, as shown in Figure 3E. Figure 3F shows that all currents in response to increments in luminance were statistically zero in the presence of APB, and all currents in response to decrements in luminance were actually less than control.

These measurements show that the LED receives no tonic input from OFF bipolars under constant background illumination, suggesting that the OFF bipolar input is strongly rectified. The reduction in OFF current under APB perfusion was unexpected and suggests a nonlinear interaction between the two systems during decrements in luminance.

Inhibition Enhances Representation of Luminance Edges.

The LED shows strong enhancement of the excitatory response to a flashed edge [33, 34]. This effect could be generated by horizontal cell-mediated surround antagonism, amacrine cell surround feedback inhibition, or both. What retinal circuitry mediates this enhancement? To answer this, we used a raster stimulus [33, 34] to assess the response of the cell at an edge. This stimulus consisted of a flashed dark square for 1 second at 21 locations across the receptive field of the LED (Figure 4A). Excitatory recordings were collected (Figure 4B) and stacked into a space-time heat map (Figure 4C).

The strong edge selectivity of excitation seen in Roska et al. [33, 34] was reproduced (Figure 5A), with locations on the inside of the edge producing a vigorous response, and locations distal from the edge being highly attenuated. Upon blockage of all common forms of retinal inhibition (GABAa with SR95531, GABAc with TPMPA, and glycine with strychnine), edge selectivity was strongly attenuated, giving a stronger response at all locations (Figure 5B). We took the ratio of average currents for areas located proximally versus distally to the edge to yield a measure of this "edge selectivity." Under control conditions, the LED had an edge selectivity of 2.72, whereas when inhibition is blocked, edge selectivity was only 1.33. This indicated that either one or all of the blocked inhibitory systems are responsible for producing a nearly 2-fold increase in edge selectivity, presumably via an inner plexiform-originated feedback pathway. A putative circuit is illustrated in Figure 5C; LEDs located distally from the edge (location 1) receive more amacrine cell-mediated feedback inhibition and their excitation is attenuated more than those located proximally (location 2).

Another qualitative difference between control-blocked and inhibition-blocked rasters was the appearance of currents on the outside of the edge at the offset of the stimulus (Figures 5A and 5B, location 3). Presumably, this excitation was generated by horizontal cells via one of the two possible mechanisms underlying surround antagonism described by Kamermans et al. and Hirasawa et al. [22, 23], whereby cone glutamate output is modulated by surround luminance; increments cause an increase in glutamatergic release, and decrements cause a decrease. Figure 5C suggests how this signal is normally eliminated by feedback inhibition.

Feedback Inhibition Originates from the Inner Plexiform Layer and Uses both GABAa and GABAc Systems.

The pharmacology of the previous result suggests that this inhibition originates in the inner plexiform layer, likely from a population of inhibitory amacrine cells. However, the results of earlier studies showed positive staining for GABA receptors at the dendrites of mammalian bipolar cells [53, 54] and horizontal cells [55], pointing to a possible feedforward role of GABA in the outer retina. To distinguish between inner and outer retina antagonism, we implemented stimuli designed to bypass the horizontal cell layer.

We stimulated the cell by driving the center with either a bright (+300% luminance) or dark (-100% luminance) 150-µm spot to elicit excitation from the OFF and ON systems, respectively (Figure 6A). This 150 µm dimension was the measured peak value of excitation in response to spots of increasing size for both OFF and ON, indicating it as the center of the LED's

excitatory receptive field (Figure 3A). We also stimulated the surround using a flipping grating with a stripe width of 50 μm, a dimension below the feature sensitivity of horizontal cells [56-61]. The ensemble of stripes was luminance-neutral, thus eliciting no response in horizontal cells. An illustration of the feedback inhibition circuit is shown in Figure 6B, with example current traces for center only (spot) and center plus surround stimulation shown in Figure 6C. Center plus surround currents were divided by center only currents and subtracted from 1 to obtain a measure of the percent reduction in current shown in Figures 6D for OFF center and 6E for ON center.

To determine the neurotransmitter systems used by feedback inhibition, we presented these stimuli under various combinations of pharmacologic blockers. We blocked GABAa with SR95531 alone, GABAc with TPMPA alone, or with both. For the OFF system, we observed an average reduction of 60.5 ± 4.6% (n=20, $P < .01$) due to feedback inhibition under control conditions. When blocking only the GABAa system, the reduction was only 37.0% ± 4.7% (n=9, $P < .01$); when blocking the GABAc systems, the reduction was 52.7% ± 5.3% (n=7, $P < .01$). Each of these measurements was significantly different than when both GABAa and GABAc were blocked (Figure 6D, 19.6 ± 6.0%; $P < .01$, $P < .03$, $P < .01$).

The ON system showed similar results, with reduction under control conditions of 61.2 ± 3.6% (n=20, $P < .01$), under GABAa blockage a reduction of 50.7 ± 9.3% (n=8, $P < .01$), and under GABAc blockage a reduction of 37.8 ± 9.9% (n=9, $P < .01$). As with the OFF system, these measurements were also significantly different than when both GABAa and GABAc were blocked (Figure 6E, 11.8 ± 9.3%; $P < .01$).

Differences in current reductions produced by each individual drug condition compared with control shows the pharmacology of the OFF and ON systems. For the OFF system, GABAa blockage was significantly different than control ($P < .01$), but GABAc blockage was not ($P = .44$). For the ON system, the opposite was true; GABAa blockage was not significantly different ($P = .21$), but GABAc blockage was ($P < .01$). This suggests that feedback inhibition to the OFF system was mediated more by GABAa, and feedback inhibition to the ON system was mediated more by GABAc. However, blockage of GABAa or GABAc individually did not cause complete elimination of feedback inhibition, nor were the current changes additive. This suggests a possible redundant contribution by both systems.

Full activation of feedback inhibition caused approximately a 60% reduction of excitatory currents. This effect was mostly alleviated by pharmacologic blockage of both GABAa and GABAc systems, but rescue of current did not appear to be complete. This suggests that another inhibitory pathway, possibly one including glycine, may also be present in feedback inhibition. However, this residual current reduction was not significant in either the OFF system ($P = .31$) or the ON system ($P = .41$). Blockage of glycine using strychnine (1 μM) also did not show any difference compared to control conditions in OFF ($P = .85$) or ON ($P = .07$) systems. This shows that feedback inhibition is exclusively mediated by GABA.

Lateral Inhibitory Feedback Components for the ON and OFF Pathways Have a Spatial Extent of 750 μm.

We used a version of this same grating stimulus (Figure 6A) in which the area of flipping grating was varied progressively from 200 μm to 1500 μm, activating different amounts of surround area. Data in Figure 6F show a linear attenuation of 50% to 60% in excitatory currents up to 750 μm. Specifically, attenuation of 52.8 ± 4.3% (n=20, $P < .01$) occurred for the OFF

system, and attenuation of 58.8 ± 4.5% (n=17, $P < .01$) occurred for the ON system, beyond which further reductions in current seem apparent but are no longer statistically significant. Thus, for OFF and ON systems, 750 µm is the spatial extent of effective feedback inhibition, which is approximately five times the size of the receptive field center.

Inhibition and Excitation are Generated by Receptive Field Subunits.

The stimuli used in Figure 6 utilized 50 µm gratings to drive feedback inhibition. This shows that feedback inhibition, in addition to being responsive to luminance changes, is also sensitive to fine detail, most likely driven by individual bipolar cells, which constitute functional "subunits" of the receptive field. We were interested to know if excitation also had similar spatial tuning characteristics. Inward currents are elicited at both increments and decrements in luminance [33, 34, 49], making it possible that the LED could sense detail much smaller than its receptive field, driven by nonlinear bipolar cells. Other studies have shown this by presenting high spatial-frequency gratings to the receptive field of a target cell and still recording excitatory input although there is no net luminance change [56, 62, 63, 57, 64]. In a receptive field driven by linear (nonrectified) bipolar cells, increases in excitatory input caused by stripes of one luminance (e.g., bright stripes stimulating the ON bipolar response) would be canceled out by decreases in excitation from the same class of bipolar cells reacting to adjacent stripes of the opposite luminance (e.g., dark stripes attenuating the ON bipolar response).

To test the ability of the LED to respond to subunits, we designed a luminance-neutral flipping grating stimulus (Figure 7A) that was restricted to the center of the LED's receptive field (150 µm). Stripe widths varied from 10 to 70 µm to measure the spatial tuning properties of excitation (Figure 7B) and feedforward inhibition (Figure 7C). Both excitation and inhibition responded to detail sizes as small as 20 µm ($P < .05$ for both). Response magnitude increased in a sigmoidal fashion up to 40 µm. At this stripe size and above, excitation produced an average change in current for the duration of the stimulus (versus baseline) of -87.1 ± 9.0 pA (n=8, $P < .01$). Feedforward inhibition produced an average current change of 110.72 ± 16.07 pA (n=10, $P < .01$). This observed 20-µm threshold size is approximately that of a typical bipolar cell dendritic field in the rabbit retina [65, 66]. These data show that LED excitation and feedforward inhibition at the receptive field center responded to features as small as one-eighth the size (20 µm) of its already small receptive field (150 µm) and responded maximally to features one-fourth the size (40 µm).

To ensure that feedforward inhibition to the LED was not cancelling out excitation, we also measured spike recordings to these same stimuli (Figure 7D). We observed average peak spike rates of 25-30 Hz for all stripe sizes larger than 40 µm, and spiking was elicited as low as 20 µm, mirroring the results seen for excitation.

Excitation Is Not Attenuated by Crossover Inhibition.

There exists the possibility that the ON and OFF systems could be interacting in such a way that reduces their responsiveness to subreceptive field detail. Molnar and Werblin [67] observed so-called "crossover inhibition", where some subclasses of bipolar cells inhibit each other though glycinergic and GABAergic amacrine cells (Figure 7E). If ON and OFF bipolar cells are activated in close proximity to one another (as would be the case with high spatial-frequency gratings), it is possible that crossover inhibition would cause mutual attenuation of excitatory currents. To eliminate this possibility, we compared recordings for the 50-µm stripe size under control conditions and all inhibition blocked (GABAa, GABAc, and glycine). We

found no change in excitatory currents (Figure 7F). If crossover inhibition were present, we would expect to see an increase during blockage. This shows that the LED probably receives input from a subtype of bipolar cells which do not interact with each other through inhibition. Otherwise, this would serve to linearize cell responses, causing it to respond only to changes in net luminance over the receptive field center. This further shows that the LED circuitry is optimized to detect fine details.

An mGluR6-Dependent Current is Generated in Response to Decrements in Luminance That Contain Fine Detail.

To assess the contribution of the OFF and ON systems during stimulation with subreceptive-field detail, we eliminated the ON system with APB (an mGluR6 agonist) while stimulating with 50 µm flipping gratings. Surprisingly, we found that there was no significant reduction in overall current (n=5, $P = .46$) (Figure 8A), meaning that there is no observable ON excitation in response to luminance-neutral stripes (i.e., the ON bipolar system is not responsive to fine detail). ON excitation does confer sensitivity to fine detail, but through an unexpected route. When presenting only dark stripes (Figure 8B), we found much larger currents than when the ON system was eliminated (n=5, $P < .01$). This shows that under control conditions, the ON system was contributing current in response to a dark stimulus. Response to presentation of only bright stripes (Figure 8C) was eliminated by APB as expected. 8D illustrates a possible mechanism for the creation of mGluR6-dependent currents by dark stripes (Figure 8B). These data show that the ON system boosts the responsiveness of the LED to fine detail that is net darker than average background luminance through ON bipolar cells, as suggested by Figure 8B.

Glycine Enhances Center Excitation by Suppressing GABAergic Feedback Inhibition.

Feedback inhibition magnitude is uneven across its receptive field as indicated in Figure 6F; locations proximal to the center give greater attenuation of excitation than those more distal. An anticipated consequence of this is that feedback inhibition is strongest at the LED center, and would cancel out a large amount of excitation, even though the surround is not being activated. Figure 9 shows that the LED is counteracting this. Figure 9A is an average recording used for calculations in Figure 9B. For both the OFF (Figure 9B) and ON (Figure 9C) systems, eliminating GABA via blockage with SR95531 and TPMPA showed no change in current elicited from a single OFF or ON spot restricted to the center for OFF (n=8, $P = .88$) or ON (n=8, $P = .35$) spots. This indicates that GABAergic feedback inhibition has no significant effect in the center, even though one would expect this location to give the strongest amount of inhibition per unit of area.

On addition of strychnine (average recording shown in 9D), we observed a large decrease in current level (Figure 9E and Figure 9F; n=8, $P < .01$ for both OFF and ON), which can be subsequently rescued via blockage of GABA to restore current levels to control (Figure 9E and Figure 9F; n=8, $P = .88$ for OFF, $P = .06$ for ON). Figure 9G illustrates this inhibition-of-inhibition interaction. If glycine, under normal conditions, is suppressing GABAergic inhibition to bipolar cells in the center, then its elimination via strychnine would cause an upregulation of GABA, leading to reduced excitatory currents. If GABA is then blocked, there is no longer any direct inhibition of excitation, which is observed as a resultant rescue of its current levels.

Feedback Inhibition Enhances Representation of Textured Edges.

As shown thus far, feedback inhibition can be activated by luminance-neutral fine detail

(features that are sized similar to bipolar dendritic fields) and can also be activated in proportion to the amount of surround area stimulated. LEDs should then respond differently to areas of active texture, depending on their distance from an edge (in this case, a border delineating an area of nontexture). Presumably, cells located close to a textured edge would receive less feedback inhibition than those located more distally, as in Figure 5.

Figure 10A shows a set of excitatory responses elicited by a luminance-neutral flashed square consisting of 50-µm stripes drifted at 1 Hz for 2 seconds, and constructed into a heat map in the same way as the raster in Figure 4. Excitatory response to this stimulus is similar to that in Figure 5A, with selectivity proximal to the edge. Spiking also shows a strong response near the edge for the initial first second of the stimulus (Figure 10B). Summing spikes at the various spatial locations for 8 cells show a nearly 2-fold preference for the edge location and indicate that the LED delivers a spiking output responsive to textured edges and reliably transmits the nearly 2-fold edge selectivity produced by feedback inhibition (Figures 5A and 5B).

To confirm that selectivity to textured edges is not elicited exclusively under carefully controlled stimulus conditions, we presented a 16-second movie that contains natural scenes while recording excitatory currents (Figure 10C). The role of feedback inhibition was also assessed by blocking GABA. The peak excitatory response for the entire movie was elicited at frame 120 (Figure 10C, right picture), where feedback inhibition also had little effect. At this time, the center of the receptive field (inner circle) contained a large degree of fine detail (insert). This area was also located near an edge; features in the surround (outer circle) below and to the left of the center were of uniform luminance and had little texture, presumably preventing any ambient jitter in the filming from eliciting feedback inhibition. The highest difference between control and GABA-blocked excitatory currents occurred at frame 55 (Figure 10C, left picture), when a car moved from right to left through the entire receptive field. This type of scene feature would elicit a large excitatory current due to the large amount of detail stimulating the center, but was subsequently suppressed by feedback inhibition which was sensitive to similar features.

Natural stimuli illustrate when LED circuitry generates the most excitation and feedback inhibition under normal visual conditions as observed by the animal. Excitation was greatest at an edge of fine detail, and feedback inhibition was most effective when non-edge bearing objects appeared in the receptive field.

Center and Surround Monotonically Encode Contrast. Center-Surround Interaction is Nonlinear.

We used a set of grating stimuli that displayed differing levels of stripe contrast For example, a 40% contrast level corresponds to a set of stripes with dark bars of -40% luminance, and light bars of +40% luminance. We generated six levels of contrast (0%, 20%, 40%, 60%, 80% and 100%) in all combinations for center (150 µm) and surround (150-1000 µm) area, giving 36 distinct combinations (Figure 11A). All combinations were displayed to the LED as 2 Hz flipping gratings, excitatory currents recorded, averaged, and normalized against the maximum recording and plotted as a heat map (Figure 11B, right).

Figure 11B shows how center and surround independently respond to contrast levels. The center shows higher excitatory responses to higher levels of contrast. According to these measurements, contrasts as low as 40% can be significantly detected by the LED excitatory system. Likewise, when center contrast is fixed at 100% and surround contrast is varied, higher levels of surround contrast cause a greater suppression of excitation. Contrasts as low as 40% can also be significantly detected.

The heat map plot suggests how feedback inhibition interacts with bipolar terminals. To test for a linear relationship, we constructed a linear equation that increases excitation with center contrast, and is linearly attenuated by an increasing amount of surround contrast. We then optimized slope coefficients for each axis (Figure 11C). This model gave a variance error value of 0.0244, indicating a fairly good fit.

We suspected this since the response to center contrast values has a concave shape, that the interaction could be nonlinear, so we added polynomial exponents to the original linear model and optimized again, giving a substantially lower variance of 0.0025, having a surround exponent of 1.25, and a center exponent of 2.13. This indicates that the center response to contrast is nonlinear, whereas the effect of surround feedback inhibition approximates a linear attenuation of center excitation.

Computational Model of Feedback Inhibition Suggests Noise Suppression Function

Single-cell patch-clamp electrophysiology has a low informational throughput, in addition to other practical limitations related to carrying out extended experiments. To get a broader view of how LED circuitry processes the visual scene, we designed a Matlab model of the interaction between feedback inhibition and excitation. The model was operated by assuming each pixel to be equivalent to the receptive field of a single bipolar cell (approximately 50 µm). Excitation and feedback inhibition responses were generated by subtracting luminance changes from a pixel-by-pixel exponential moving average of luminance (luminance differential matrix), played at 30 frames/sec. Currents elicited by spots were fit to an exponential moving average, with alpha constants numerically optimized to recorded data (excitation_alpha = 0.1, feedback_alpha = 0.2). Amount of surround activation was determined by convolving a normalized two-dimensional Gaussian (sigma = 250 µm, derived from Figure 6F) with the luminance differential matrix for feedback inhibition. The resulting level of excitatory output at each pixel was then determined by using the center-surround contrast plot in Figure 11A as a lookup table to obtain the appropriate fraction of excitatory activation, and multiplying by a value of 50 pA. A 'raw' version of excitation was created by fixing the value of feedback inhibition at a constant of zero.

Figure 12A shows an example frame of inhibited excitation, raw excitation, the original frame from which they were derived, and a subtractive difference between them. Qualitatively, the inhibited excitation appears to contain a more sparse representation of the edges compared to raw. The difference image verifies this by showing a somewhat diffuse version of the original image. Since diffuseness implies having low spatial frequencies, we performed sequential fast Fourier transforms on simulated excitatory outputs, and converted spatial dimensions to visual degrees (160 µm = 1° visual angle [68]). Figure 12B is the ‘inhibited’ power spectrum divided by the ‘raw’ power spectrum, which shows the spatial frequencies that feedback inhibition selects for. All spatial frequencies are attenuated by at least 30%, but large spatial frequencies (0.25 cycles/° visual angle) are selectively attenuated.

To test the sparseness of the 'inhibited' signal, we created binned distributions of the simulated excitatory values for the 'inhibited' and 'raw' data sets, ranging from 0 to 50 pA, with a bin size of 0.1 pA. Figure 12C was created by dividing the 'inhibited' distribution by the 'raw' distribution, and displaying as a log plot. Since all pixels created by this simulation must have some value between 0 and 50, this plot illustrates how they become preferentially distributed when feedback inhibition is enabled. Current values that are above log 1 have their quantity enhanced, and those below 1 are attenuated in quantity. The value representing 0 pA is greater

than log 1, meaning the amount of 'bipolars' that generate no excitatory current increases nearly 10-fold in the presence of feedback inhibition, essentially increasing the amount of 'blank space', or sparseness in the scene. The green area in Figure 12C illustrates the redistribution of bipolar excitatory values from various nonzero current values (below the log 1 line) to zero current values (above the log 1 line). This is what we would expect from a feedback inhibition that is shunting in nature.

We also compared Shannon Entropy measurements between the data sets. Each frame was normalized by scaling the full range to 16-bits. Entropy is a measurement of the amount of uncertainty contained in an image [69], with perfect uniform noise having an entropy value of 16 for a 16 bit image. Changes in this metric of disorder are often used to measure the change in information transfer content of neurological systems, with decreasing entropy equating to an increase in information content [70-73]. Data show that feedback inhibition decreases the amount of uncertainty in the bipolar representation of a scene from an entropy value of 5.51 ± 0.56 bits to 5.16 ± 0.50 bits (n = 30, $P < .05$) (Figure 12E). Feedback inhibition also causes a decrease the sparseness index (thereby increasing sparseness, see Zeck et. al [47]) to 0.427 ± 0.082, from 0.502 ± 0.049 (n = 30, $P < .05$) (Figure 12D), meaning that there is a higher ratio of silence to signal across the entire distribution of response. The difference image also had a sparseness on par with the raw image (0.514 ± 0.515), but had a larger standard deviation, possibly reflecting the transient nature of feedback inhibition.

Since metrics of entropy and sparseness are generated via a computational model, it follows that the difference between two populations may be small, but still gives a high degree of statistical significance due to low variance in the sample. Descriptive statistics give a clearer picture of how important these measured differences are. We calculated the Cohen's *d* effect size for sparseness and entropy measurements [74]. The change in sparseness due to the presence or lack of feedback inhibition (Figure 12D) had an effect size of 0.902, considered to be large for this type of statistic [74]. The effect size of the change in entropy (Figure 12E), was smaller but still substantial at 0.640. These results show that feedback inhibition serves to make signals in the scene more sparse, and improve the information content by lowering entropy.

Feedforward Inhibition Is Glycinergic and Can Signal Rapid Narrow Luminance Changes.

Comparing feedforward inhibition's response to spots of excitation, it appears that feedforward inhibition is most active at the moment of onset or offset of stimuli, likely the basis for van Wyk et al's. [49] suggestion that feedforward inhibition could primarily be used to delay spiking by "blanking out" select early phases of excitation.

Selective blockage via strychnine could be used to measure the influence of feedforward inhibition. However, strychnine perfusion eliminates not only feedforward inhibition, but also drastically changes and attenuates the waveforms of OFF and ON excitation (as seen in Figure 9D). It is therefore difficult to determine what the specific effect of feedforward inhibition is upon cell response via pharmacology. We therefore worked to find specific stimulus conditions that would function to block spiking, because spiking has been preserved thus far in most stimuli used in this study, in spite of feedforward inhibition being present.

We investigated the interaction of excitation and feedforward inhibition by recording responses to stimuli designed to elicit a baseline spike rate by presenting a 50-µm drifting grating in the 150-µm center drifted at 1 Hz. We then superimposed rapid luminance shifts with a single 133-ms flash of either a narrow (150-µm) or wide (1000-µm) spot during the drifting grating, as indicated by grey bars (Figures 13A-13F). During each drifting grating, both excitation and

inhibition were active, yet a constant spike train was produced. The spike train was interrupted during each luminance shift condition.

The interaction mediating this interruption was different for narrow and wide flashes. For narrow OFF or ON flashes (Figures 13C and 13E), an additional wave of feedforward inhibition was produced on top of the baseline elicited by the drifting grating. This inhibition then postsynaptically canceled the excitatory current, producing a shutoff of spiking. For wide flashes (Figures 13D and 13F), feedforward inhibition was barely affected. Instead, the spike train was shut off by a reduction in excitation, presumably aided by a combination of horizontal antagonism and feedback inhibition.

Figure 13G shows the measured half-maximum rise and fall times of OFF (left) and ON (right) feedforward inhibition. In both cases, the current took 4 to 5 times longer to decay than to reach its peak.

Furthermore, the pharmacology of feedforward inhibition was determined. Strychnine (1 μM) was perfused with the media while recording inhibitory currents in response to 200 μm OFF and ON spots. Figure 13H shows that strychnine eliminates inhibitory currents. Excitatory currents were also recorded to ensure cell viability (not shown).

Figure 13I is an illustration of how feedforward inhibition's sensitivity to fine detail (Figure 7C) and differences in rise and decay times (Figure 13G) contribute to producing the inhibitory waves observed in Figures 13C and 13E, as explained in the discussion.

DISCUSSION

We have shown that the LED has several circuit characteristics that enhance sensitivity to fine detail, and allow surround activity to strongly suppress center activity. When combined together, we get a view of the exact neuronal underpinnings that the retina uses to solve the problem of edge representation. Which neurotransmitter systems are employed, and in which synaptic layers is the primary contribution of this work. Even though complex center-surround antagonism was suggested by earlier studies [48, 49], they made no distinction between outer plexiform-driven and inner plexiform-driven circuitry. The van Wyk study in particular concluded that larger grating sizes more effectively suppressed center-generated spiking. This can be explained by the fact that the spatial features used were large enough to activate outer plexiform circuitry and were not designed to avoid luminance changes that could drive horizontal cells. These stimuli likely elicited antagonism originating in both the inner and outer plexiform layers. In this study, stimuli specifically avoided activating horizontal cell circuitry by using luminance-neutral gratings of spatial resolution that were too fine to activate horizontal cells. This enabled us to define inner plexiform components of inhibition that were unique to the LED.

Summary of Synaptic Pathways Mediating Local Edge Detector Activity

Figure 14A outlines the circuitry derived from our measurements. Populations of ON and OFF bipolar cells (a, b) converge upon the LED. Small dendritic extent and nonlinear synaptic inputs endow the LED with high spatial sensitivity. These bipolar cells (or other classes of bipolar cells) make excitatory contact with ON-OFF narrow-field glycinergic amacrine cells (j, k), ganglion cell dendrites (c, d) and wide-field amacrine cells, so all components have high spatial sensitivity. Excitatory inputs to the ganglion cell are rectified. This rectification, likely present in the bipolar-to-amacrine cell connections as well, is essential for the high spatial resolution in the inhibitory responses: glycinergic feedforward (e, f) and feedback from GABAa (h) and GABAc (g). Feedback is in the center inhibited by a glycinergic source (l, m).

Feedback Inhibition

Figure 5A suggests that the LED is performing classic luminance edge-detection. According to Marr and Hildreth [15], ideal edge detection can be achieved by applying a difference-of-Gaussian function to a scene, where the sigma values of each Gaussian approximate each other but are not exactly the same. This type of difference-of-Gaussian creates the familiar “Mexican hat” receptive field of ganglion cells described in classic works, also known as a Laplacian function [75, 76] (Figure 1C). This function shows that the presence of a strong antagonistic surround is necessary to create sufficient edge detection. In the LED, this component is provided by GABAergic feedback inhibition originating from inner plexiform amacrine cells, as shown in Figure 6. However, sufficiently strong excitation is also necessary, and one possible problematic consequence of having strong local feedback inhibition is that center excitation would be attenuated heavily, since presumably this is where feedback inhibition is the strongest, as suggested by Figure 6F. The LED appears to counteract this by using glycinergic inhibition to suppress GABAergic feedback inhibition cospatially with the excitatory center (Figure 9). Thus, glycinergic and GABAergic inhibition combine in such a way that approximates a Laplacian function by creating a strong center combined with a strong antagonistic surround.

We found that both GABAa and GABAc systems are utilized in signaling feedback inhibition, with GABAa mostly suppressing the OFF system, and GABAc mostly suppressing the ON system. Paradoxically, blockage of either of these primary systems produced only a partial restoration of current, suggesting that perhaps both GABAa and GABAc might be present at both ON and OFF bipolar cell terminals. The sub-linear summation of each receptor isotype's contribution (Figure 6D and 6E) suggests some functional redundancy. Besides redundancy, combining these two isotypes in different proportions can tune the kinetic properties of feedback inhibition, due to the fast and slow nature of GABAa and GABAc, respectively [77-79]. This would either imply that the temporal response of feedback inhibition to bipolar cells is carefully tuned to have an optimal time course, or that each system is performing a specific role in space or time. This is entirely plausible given that spatial segregation at synaptic clefts is sufficient to prevent signal cross-talk [80]. Further work is required to determine the possible sub-functionality of feedback inhibition.

How feedback inhibition and excitation encode contrast also warrants discussion. Both center and surround encode contrast levels monotonically – larger center contrasts increase excitation, larger surround contrasts decrease this excitation (Figure 11B). The relationship between the levels of contrast and the amount of excitation produced by each contrast level was found to conform somewhat to a linear expression. However, adding exponents (thereby making the relationship nonlinear) produced a better fit upon optimization, with excitation having a rather large polynomial exponent of 2.13. This means that excitation levels increased to the *square* of contrast. This would seem counter to studies which have shown excitatory responses to undergo contrast gain control, thereby attenuating the amount of increase in excitation when increasing contrast at already high levels [81-83]. This would seem to imply that LED bipolars have a positive contrast gain factor. Since this nonlinearity also seems to be present in response to dark spots of increasing intensity (i.e. lower luminance, Figure 3E), this is probably a feature of the OFF system. There are several possible sources of this nonlinearity. It is unlikely originated in either the photoreceptor-to-bipolar cell synapse or within the dendrites of the bipolar cell, since OFF bipolar cell voltage and current responses saturate at low luminance changes [84]. It is also unlikely to be regulated by an inhibitory amacrine cell since blockage has no effect upon absolute current levels elicited by high contrast gratings (Figure 7F) or spots (Figures 9E and 9F). The only remaining possible sources of nonlinearities are either the bipolar terminal or the bipolar cell-to-ganglion cell synapse. In the first case, one cannot rule out intrinsic voltage or calcium-dependent properties that could produce an internal positive feedback for vesicle release. In the second case, mGluRs at the ganglion cell dendrites could produce an excitatory signal amplification. Indeed, mGluRs are present in ganglion cell dendrites [85-87], but their role in retinal signal processing has not been extensively studied. The surround had a polynomial exponent of 1.25, which is close to being linear. This allows us to describe the center-surround relationship as being a linear attenuation by feedback inhibition of an already nonlinear center.

Sensitivity to Fine Detail

OFF and ON excitation are rectified, meaning OFF bipolar cells generate no significant reduction in glutamate release in response to increments in light, and ON bipolar cells generate no significant reduction in glutamate release in response to decrements of light. If both OFF and ON bipolar cell inputs were perfectly non-rectified (i.e. having a linear response to luminance changes), then inward currents from each phase would be cancelled out by equal and opposite

(outward) currents from the other system (Figure 3D), thereby making the receptive field center linear [41]. Because of the apparent rectification, we deduced that bipolar cell subunits could contribute independently to excitation and confer responsiveness to subreceptive field detail, provided the two systems don't actively inhibit each other. In some subclasses of bipolar cells, inhibition can be generated by amacrine cells driven by the ON system to suppress OFF excitation, or vice-versa [67]. The lack of this type of inhibition (Figure 7F) in these bipolar cells confers the functional advantage of enhanced responsiveness to fine detail.

Furthermore, even though ON excitation makes no direct contribution in response to fine detail, it contributes in another way: ON bipolar cells generate an excitatory current when there is a *decrement* in net luminance, so long as there are areas of neutral luminance contained in the stimulus. This seemingly paradoxical response can be explained by the circuitry shown in Figure 8D; horizontal cells cannot respond to 50-μm features but are activated by luminance changes. Thus, horizontal cells are activated by the net decrement in luminance provided by the dark bars in Figure 8B, which in turn feed back to cones underneath the neutral (grey) bars by either a pH-mediated or hemichannel-mediated emphatic mechanism [22, 23]. This induces these cone photoreceptors to release less glutamate, which then elicits excitation from mGluR6-bearing ON bipolar cells. Thus, ON bipolar cell responsiveness to fine detail is conferred via horizontal cells, and the mere presence of ON bipolar cells to LED synapses boosts response to fine detail under decrements in luminance.

We uncovered this same horizontal cell mechanism upon elimination of inhibition during edge stimuli (Figure 5B, area 3); the disappearance of the large dark square during the stimulus drove horizontal cells in the surround, that in turn increased the level of glutamate release at cone terminals in the center, which consequently induced an OFF current. This suggests a secondary role of feedback inhibition in the context of luminance edges: the elimination of erroneous horizontal cell signals that could potentially give a false signal of the location of the edge in time and space. Figure 5D illustrates how this signal is eliminated. Since the offset of a dark square is seen as an increment in luminance, ON bipolar cells located in the surround respond to this increment by increasing glutamate output, driving feedback inhibition, and subsequently blocking the excitatory current generated by the horizontal cell system.

Complex receptive field properties further enhance the edge-detection capabilities of the LED beyond the detection of just luminance edges. Subreceptive field resolution is created by rectified excitation from bipolar cells, thereby making the receptive field nonlinear [41]. This effect has also been measured in the immediate surround of the Y (alpha) cell [56, 64], theoretically enabling the cell to represent textured areas. Yet the addition of a similarly texture-sensitive feedback inhibition causes cell populations to represent the *boundaries* of textured areas instead, as shown in Figure 10A. A generalized mechanism of textured edge detection is illustrated in Figure 14B. A large area containing subunit-sized detail drives both excitation and feedback inhibition. Because excitation has a smaller receptive field than feedback inhibition, its representation of the area is sharp, whereas inhibitory feedback is more diffuse. Excitation and feedback inhibition sum in the Laplacian manner (as described above) at the bipolar cell terminal, but each circuit component represents *variance* in luminance rather than luminance contained in its receptive field. This allows the border of the textured area to be encoded, which we suggest is an added functionality of feedback inhibition.

Textured edge detection has possible implications for behavior. Cuthill et al. [1] showed that targets can be effectively camouflaged from avian predators by using background-matched texture over the entirety of their surface. However, when the coloration pattern was statistically

altered so no texture contacted the inside edge, recognition of the target significantly improved, meaning that a border between a textured area (tree bark) and a uniform area (the target's inside edge) was perceived. We postulate that the feedback inhibition circuitry in the LED makes this type of behavior possible, because it allows the differentiation between a textured and non-textured area, regardless of luminance differentials. Figure 10C demonstrates the LED's capacity to perform this function in a natural scene; excitation peaked at textured areas bordering featureless smooth areas, and feedback inhibition was most effective at suppressing excitation during the presence of features that did not resemble borders.

It should be noted that textured edge enhancement in both designed and natural stimuli involve feature motion. This suggests that both natural object motion and small saccades might play a role in LED function and subsequent perception of complex borders. Indeed, many circuit components seem to be tuned for high sensitivity to fine spatial detail, but this study only resolved this characteristic at temporal frequencies of about 2 Hz. How eye movements and natural object motion impact complex edge representation are questions that warrant further study.

Information and Noise

Comparison of simulated excitation that receives feedback inhibition versus raw excitation shows that feedback inhibition induces a distinct change in the content and character of excitation. Sparseness and information content increase, while Fourier analysis upon the spatial domain shows a selective attenuation of large features.

An index of sparseness was created to compare two ganglion cell types by Zeck et. al [47]. This index is simply a measurement of how many active pixels are next to any given pixel in the scene (thus a lower sparseness index indicates a higher level sparseness). The functional meaning of high sparseness is that the signal is highly specific to a certain type of stimulus, and will be unresponsive to irrelevant patterns, thus indicating a highly specialized information channel. Here we show that feedback inhibition is the key component in generating this behavior. Indeed, Figure 5 alone is a testament to feedback inhibition's ability to remove response in what is essentially an informationally 'blank' area – area devoid of an edge.

Upon inspection of the 'difference' image (in Figure 12A), it becomes apparent that what's being removed has the characteristic of being spatially broad (low frequency). This outcome can be directly related to what is seen in Figure 6 – essentially any point in space that has a large number of activated neighbors has a high chance of being attenuated. While not 'noise' in the classical engineering sense, this particular scene content is being dispensed with via the LED circuitry while retaining essential content. This is the very definition of an entropic decrease, since lower bandwidth (fewer 'bits') is needed to encode the scene. This result conceptually agrees with studies showing that sluggish cells have relatively low informational throughput [88].

The Effect of Feedforward Inhibition on Spiking

Feedforward inhibition was found to be ON-OFF, to be responsive to subreceptive field detail, and to have a receptive field peak of 150 μm, similar to excitation. What is the purpose of such a circuit component if it cancels out excitation? Van Wyk et al. [49] observed that feedforward inhibition is more transient than excitation, delaying the onset of spiking, and making the cell response more sluggish. This mechanism might ensure that scene features are not detected until they have been fixed on the retina for about 150 msec. Here we suggest an

additional function. Figure 13A shows that feedforward inhibition is active even during narrow-field stimulation by a drifting grating. Spiking still persists, however, suggesting that inhibition suppresses spiking under conditions other than responses to a test flash. Spiking was suppressed during an instantaneous change in narrow-field luminance, which we term an "edge in time." During this shift, the receptive field subunit response of feedforward inhibition (Figure 7C) suppresses spiking as illustrated in Figure 13I. During a drifting grating, ON or OFF subunits (inside the dotted orange circle) are either active (in this case, the ON subunit) or inactive (the OFF subunit). At the moment of shift (grey bar), all OFF subunits respond to the decrement in luminance. Because the rise time of feedforward inhibition is faster than the decay time (Figure 13G), both ON and OFF feedforward inhibition are active at this instant, adding to produce a wave of inhibition on top of the baseline. This inhibition is enough to block spiking, as indicated in Figures 13C and 13E.

What is the purpose of momentarily blanking the LED's spike train? It is possible that during times of constant spiking, blank periods might encode information. This mechanism has been suggested in cerebellar Purkinje cells, where the duration of a pause contributed to distinguishing between inputted patterns [89, 90]. Whether the LED's target can meaningfully decode these blanked periods is unknown. Given the limited number of axons that can fit into the optic nerve, it is plausible that several informational channels could be compressed into a single set of axon tracts. Because sluggish cells have slow informational throughput in terms of measured spikes [88], perhaps feedforward inhibition maximizes available bandwidth.

Edge detection is a process of interest to a wide range of disciplines: machine vision, organismal behavior, and psychophysics. It has also been implicated in several differing sensory modalities across vastly unrelated animal species, implying independent evolution. The LED is an example of how neurons can successfully assemble circuitry in order to extract boundaries from complex sensory input, and contribute to building perception of the physical world.

EXPERIMENTAL PROCEDURES

All procedures involving live animals were approved by the University of California Berkeley Animal Care and Use Committee, and performed in accordance with institutional guidelines. Rabbits were sacrificed and their eyes removed and hemisected as described previously [33, 34]. Segments of the visual streak along with their associated sclera were stored in oxygenated Ames medium in the dark. Individual segments were removed from the sclera and flat-mounted on Millipore paper containing a 4-mm center hole. The mounts were perfused with Ames solution at 32°C. The solution was saturated with a mixture of 95% O_2 and 5% CO_2 and pH-buffered with $NaCO_3$ to a pH of 7.4.

Patch Clamp

Local edge detectors, identified as having a sustained ON-OFF spiking pattern with loose-patch as indicated by van Wyk et al. [49], were whole-cell patch-clamped with glass electrodes with a resistance between 5 and 10 MΩ. The electrodes were filled with a cesium-based intracellular solution (in mM: 113 $CsMeSO_4$ [Sigma, St. Louis, MO, USA]; 1 $MgSO_4$ [Fisher Scientific, Pittsburgh, PA, USA]; 7.8 103 $CaCl_2$ [Fisher Scientific]; 0.5 BAPTA [1,2-bis(o-aminophenoxy)ethane-N,N,N',N'-tetraacetic acid; Fisher Scientific]; 10 HEPES [4-(2-hyrdoxyethyl)-1-piperazineethanesulfonic acid; Sigma]; 4 ATP-Na_2 [Sigma]; 0.5 GTP-Na_3 [Sigma]; 5 QX-314 [Sigma]; and 7.5 Neurobiotin-Cl [Vector Laboratories Inc, Burlingame, CA, USA], pH 7.2).

Excitatory currents were measured by voltage clamping the cell at the calculated reversal potential for chloride (-60 mV). Feedforward inhibitory currents were recorded by voltage clamping the cell at the cation reversal potential (0 mV). Since the clamp was performed at the exact reversal potential for each type of current, they were typically well isolated. The voltage response of the cell was recorded at a current clamp of 0 pA. The chloride reversal potential was confirmed by inhibitory synaptic noise, which reversed polarity at 60 mV. In most cases, excitation was recorded first, followed by voltage (under a current clamp), followed by inhibition. Recordings were digitized and sampled at 10 kHz. Signals were filtered and down-sampled to a 60-Hz sample rate, the same as the update rate of the stimulus. No meaningful signals (light-responsive or otherwise) were observed above this frequency.

Stimulus Paradigms

For each of the clamp states, several stimuli were presented against a grey background, at a brightness of 19.02 $\mu W/cm^2$, using a standard DLP projector, projecting onto a diffuser, and focused onto the photoreceptor layer via a condenser at the start of each experiment.

All -100% (OFF), +100% (ON), and +300% (ON) luminance values had brightness values of 1.08 $\mu W/cm^2$, 41.29 $\mu W/cm^2$, and 72.58 $\mu W/cm^2$, respectively. Special care was taken to make striped stimuli luminance-neutral, meaning decrements in brightness by OFF bars were offset by increments in brightness by adjacent ON bars. This ensured that blurring the image would produce no net change in luminance versus background at the diffuser. As an added measure of safety, ultrafine grating stimuli (5.7-µm stripes, presumably below the detection level of bipolars) were presented to the cell under the patch clamp, thus ensuring that no response was elicited. Gratings were also used as a static background when possible.

Edge raster plots were created by recording under the patch clamp, while sequentially displaying 1-second flashed squares at 21 spatial locations, spaced 30 µm apart, with a 5-second interstimulus rest time (Figure 4). For drifting grating rasters, the square was displayed for 2

seconds, during which time it was drifted across the display a distance of 100 µm (one full stripe cycle), reset, and drifted again. No square was visible during the interstimulus interval. Some raster stimuli were run backwards or run as a limited stimuli set with a 10-second interstimulus interval to confirm that effects were not due to rundown. A conceptual treatment of spatiotemporal rasters can be found in Roska et al. [34].

Natural scenes were recorded with a Canon PowerShot G9 digital camera, at 640 x 480 pixel resolution, 30 frames per second in black and white mode. Individual frames were converted to bitmaps, and scaled to approximate 50 visual degrees in rabbit.

Pharmacology

Experiments were repeated in the presence of pharmacologic blockers of excitation and inhibition. To block metabotropic glutamate receptors and to selectively inactivate the ON system, 20 µM 2-amino-4-phosphonobutyric acid (APB, L-AP4; Tocris Bioscience, Ellisville, MO, USA) was added to the Ames medium and perfused across the preparation. To block ionotropic GABAa or GABAc receptors, 5 µM SR95531 (Sigma) or 100 µM TPMPA ([1,2,5,6-tetrahydropyridin-4-yl]methylphosphinic acid; Tocris) was added to the Ames medium and perfused across the preparation. Recordings were performed a third time with only the Ames medium as a control when it was possible to confirm washout. To block ionotropic glycine receptors, 1 µM strychnine (Sigma) was added to the Ames medium and perfused across the preparation. The wash step was repeated, but we found that strychnine was very slow to washout and so was rarely reversible. In most instances, rundown of excitation was observed between control and drug perfusion. To compensate for this, all pharmacologic data were expressed in terms of an internal control stimulus response, often a single flashed spot.
Commonly used GABA receptor antagonists, including SR95531, also can antagonize glycine receptors (GlyRs) [91]. However, the concentration of SR95531 used in this study was much smaller (5 µM) than that required to appreciably affect GlyRs (20 µM). TPMPA does not affect GlyRs [91].

Data Analysis

All analyses were performed with Matlab R2007b (The MathWorks, Inc., Natick, MA, USA). To derive numbers corresponding to the response of a cell to a single stimulus event, the average current over the duration of the stimulus was subtracted from the recording's baseline (the statistical mode of the entire recording). For raster plots, each of the 21 stimuli events were placed sequentially side-by-side along the y-axis, with the x-axis corresponding to the 0.5 second before the stimulus, the 1-second duration of the stimulus, followed by the 0.5 second after the stimulus. Vertical bars were added to indicate the onset and offset of the stimulus. A horizontal bar was added to correspond to the point in space where the edge of the square split the middle of the cell's receptive field.

For measurements where currents were expressed as a single value (as opposed to showing a current recording), currents were first measured in response to stimuli as indicated above. The average current change was calculated by subtracting recorded values at each time from the baseline and averaging them. One value per stimulus condition per cell was generated this way. For multiple cells, average current values were averaged together, and when appropriate, statistical analyses were performed of their distribution. For normalized values, means are expressed as the proportion of the maximum average current change in a single stimulus sequence. Some cells produced peak values at different input parameters, and thus

average normalized peak values are sometimes less than 1.0.

To calculate the strength of surround inhibition, we divided the average current recorded over the duration of the center-surround stimulus (spot plus flipping gratings) by the center-only stimulus (spot only), which gives the amount of current remaining when surround stimulus is included. We then subtracted this from 1.0 and expressed as a percentage to show the current reduction. All error bars indicate an interval corresponding to the standard error of the mean (SEM). Statistical tests comparing means of populations were performed with a 2-sample *t* test. Statistical tests comparing a population mean to a specific number were performed with a 1-sample *t* test. The threshold for statistical significance was $P < .05$.

Cohen's *d* was used to calculate effect size, using pooled standard deviation from each compared sample [74].

Modeling Center-Surround Interactions

A linear center-surround interaction model fashioned after the data contained in Figure 11B was created with the following equation:

Equation 5.

$$response = (1 - m_{surround}\, contrast_{surround}) m_{center}\, contrast_{center}$$

where *m* are linear slopes, and *contrast* range from 0 to 1 in 0.2 steps. Response values were obtained using iterative values for m_{center} and $m_{surround}$. Most optimal set was determined by lowest root mean squared (RMS) value versus measured data.

A non-linear center-surround interaction model was created by inserting exponents *a* and *b* into equation 1, thereby making it a polynomial relationship:

Equation 6.

$$response = (1 - m^{a}_{surround}\, contrast_{surround}) m^{b}_{center}\, contrast_{center}$$

Response values were obtained using two stages of iterative values for m_{center} , $m_{surround}$, *a*, and *b*. Most optimal set was determined by lowest RMS value versus measured data.

REFERENCES

1. Cuthill, I. C., Stevens, M., Sheppard, J., Maddocks, T., Párraga, C. A., and Troscianko, T. S. (2005). Disruptive coloration and background pattern matching. Nature *434*, 72-74.

2. Stevens, M., and Cuthill, I. C. (2006). Disruptive coloration, crypsis and edge detection in early visual processing. Proc. Biol. Sci *273*, 2141-2147.

3. Lau, K. K., Roberts, S., Biro, D., Freeman, R., Meade, J., and Guilford, T. (2006). An edge-detection approach to investigating pigeon navigation. Journal of theoretical biology *239*, 71–78.

4. Mann, R., Armstrong, C., Meade, J., Collett, M., Guilford, T., and Roberts, S. (2008). Pigeon route learning is maximally facilitated at intermediate visual landscape edge densities. Proceedings of the Royal Institute of Navigation 2008.

5. Chait, M., Poeppel, D., and Simon, J. Z. (2008). Auditory temporal edge detection in human auditory cortex. Brain research.

6. Hofmann, M. H., Chagnaud, B. P., and Wilkens, L. A. (2009). An Edge Detection Filter Improves Spatial Resolution in the Electrosensory System of the Paddlefish. Journal of Neurophysiology, 91215–2008.

7. Newton, J., Barrett, S. F., Wilcox, M. J., and Popp, S. (2002). Biologically based machine vision: signal analysis of monopolar cells in the visual system of Musca domestica. Biomedical sciences instrumentation *38*, 123.

8. Werthmer, M. (1923). Untersuchungen zur Lehre der Gestalt, ch. 4, vol. II. Psychologische of Forschung, 301–350.

9. Hodes, L. (1961). Machine processing of line drawings. Rept. 54G-0028, MIT Lincoln Lab, Lexington, Mass.

10. Nadler, M., and Cie des Machines, B. (1963). An analog-digital character recognition system. IEEE Transactions on Electronic Computers, 814–821.

11. Sakai, T., Nagao, M., and Fujibayashi, S. (1969). Line extraction and pattern detection in a photograph. Pattern Recognition *1*, 233–248.

12. Argyle, E., and Rosenfeld, A. (1971). Techniques for edge detection. Proceedings of the IEEE *59*, 285–287.

13. Wechsler, H., and Kidode, M. (1977). A new edge detection technique and its implementation. IEEE Transactions on Systems, Man and Cybernetics *7*, 827–836.

14. Sobel, I., and Feldman, G. (1968). A 3x3 isotropic gradient operator for image processing. Presentation for Stanford Artificial Project.

15. Marr, D., and Hildreth, E. (1980). Theory of edge detection. Proc. R. Soc. Lond., B, Biol. Sci *207*, 187-217.

16. Canny, J. (1986). A computational approach to edge detection. IEEE Transactions on pattern analysis and machine intelligence, 679–698.

17. Mehrotra, R., Namuduri, K. R., and Ranganathan, N. (1992). Gabor filter-based edge detection. Pattern Recognition *25*, 1479–1494.

18. Keith Price Annotated Computer Vision Bibliography Available at: http://www.visionbib.com/bibliography/contents.html [Accessed August 29, 2009].

19. Baylor, D. A., Fuortes, M. G., and O'Bryan, P. M. (1971). Receptive fields of cones in the retina of the turtle. J. Physiol. (Lond.) *214*, 265-294.

20. Gerschenfeld, H. M., and Piccolino, M. (1980). Sustained feedback effects of L-horizontal cells on turtle cones. Proc. R. Soc. Lond., B, Biol. Sci *206*, 465-480.

21. Wu, S. M. (1991). Input-output relations of the feedback synapse between horizontal cells and cones in the tiger salamander retina. J. Neurophysiol *65*, 1197-1206.

22. Kamermans, M., Fahrenfort, I., Schultz, K., Janssen-Bienhold, U., Sjoerdsma, T., and Weiler, R. (2001). Hemichannel-mediated inhibition in the outer retina. *292*.

23. Hirasawa, H., and Kaneko, A. (2003). pH changes in the invaginating synaptic cleft mediate feedback from horizontal cells to cone photoreceptors by modulating Ca2+ channels. J. Gen. Physiol *122*, 657-671.

24. Werblin, F. S., and Dowling, J. E. (1969). Organization of the retina of the mudpuppy, Necturus maculosus. II. Intracellular recording. J. Neurophysiol *32*, 339-355.

25. DeVries, S. H. (2000). Bipolar cells use kainate and AMPA receptors to filter visual information into separate channels. Neuron *28*, 847-856.

26. Masu, M. et al. (1995). Specific deficit of the ON response in visual transmission by targeted disruption of the mGluR6 gene. Cell *80*, 757-765.

27. Ehinger, B., and Lindberg-Bauer, B. (1976). Light-evoked release of glycine from cat and rabbit retina. Brain Res *113*, 535-549.

28. Miller, R. F., Dacheux, R. F., and Frumkes, T. E. (1977). Amacrine cells in Necturus retina: evidence for independent gamma-aminobutyric acid- and glycine-releasing neurons. Science *198*, 748-750.

29. Grüsser, O. J. (1971). A quantitative analysis of spatial summation of excitation and

inhibition within the receptive field of retinal ganglion cells of cats. Vision Res *Suppl 3*, 103-127.

30. Tachibana, M., and Kaneko, A. (1988). Retinal bipolar cells receive negative feedback input from GABAergic amacrine cells. Vis. Neurosci *1*, 297-305.

31. MacNeil, M. A., Heussy, J. K., Dacheux, R. F., Raviola, E., and Masland, R. H. (2004). The population of bipolar cells in the rabbit retina. J. Comp. Neurol *472*, 73-86.

32. Wässle, H. (2004). Parallel processing in the mammalian retina. Nat. Rev. Neurosci *5*, 747-757.

33. Roska, B., and Werblin, F. (2001). Vertical interactions across ten parallel, stacked representations in the mammalian retina. Nature *410*, 583-587.

34. Roska, B., Molnar, A., and Werblin, F. S. (2006). Parallel processing in retinal ganglion cells: how integration of space-time patterns of excitation and inhibition form the spiking output. Journal of neurophysiology *95*, 3810-3822.

35. MacNeil, M. A., and Masland, R. H. (1998). Extreme diversity among amacrine cells: implications for function. Neuron *20*, 971-982.

36. MacNeil, M. A., Heussy, J. K., Dacheux, R. F., Raviola, E., and Masland, R. H. (1999). The shapes and numbers of amacrine cells: matching of photofilled with Golgi-stained cells in the rabbit retina and comparison with other mammalian species. J. Comp. Neurol *413*, 305-326.

37. Massey, S. C., O'Brien, J. J., Trexler, E. B., Li, W., Keung, J. W., Mills, S. L., and O'Brien, J. (2003). Multiple neuronal connexins in the mammalian retina. Cell Commun. Adhes *10*, 425-430.

38. Zhou, Z. J., and Lee, S. (2008). Synaptic physiology of direction selectivity in the retina. J. Physiol. (Lond.) *586*, 4371-4376.

39. Hsueh, H., Molnar, A., and Werblin, F. S. (2008). Amacrine-to-amacrine cell inhibition in the rabbit retina. J. Neurophysiol *100*, 2077-2088.

40. Rockhill, R. L., Daly, F. J., MacNeil, M. A., Brown, S. P., and Masland, R. H. (2002). The diversity of ganglion cells in a mammalian retina. J. Neurosci *22*, 3831-3843.

41. Shapley, R., and Lennie, P. (1985). Spatial frequency analysis in the visual system. Annu. Rev. Neurosci *8*, 547-583.

42. Cunningham, D. W., Shipley, T. F., and Kellman, P. J. (1998). The dynamic specification of surfaces and boundaries. Perception *27*, 403-415.

43. Elder, J. H., and Sachs, A. J. (2004). Psychophysical receptive fields of edge detection mechanisms. Vision Research *44*, 795–813.

44. Peromaa, T., and Laurinen, P. I. (2004). Separation of edge detection and brightness perception. Vision Res *44*, 1919-1925.

45. Hubel, D. H., and Wiesel, T. N. (1962). Receptive fields, binocular interaction and functional architecture in the cat's visual cortex. J. Physiol. (Lond.) *160*, 106-154.

46. Hubel, D. H., and Wiesel, T. N. (1968). Receptive fields and functional architecture of monkey striate cortex. J. Physiol. (Lond.) *195*, 215-243.

47. Zeck, G. M., Xiao, Q., and Masland, R. H. (2005). The spatial filtering properties of local edge detectors and brisk-sustained retinal ganglion cells. European Journal of Neuroscience *22*, 2016.

48. Levick, W. R. (1967). Receptive fields and trigger features of ganglion cells in the visual streak of the rabbits retina. The Journal of Physiology *188*, 285-307.

49. van Wyk, M., Taylor, W. R., and Vaney, D. I. (2006). Local edge detectors: a substrate for fine spatial vision at low temporal frequencies in rabbit retina. Journal of Neuroscience *26*, 13250.

50. Berson, D. M., Pu, M., and Famiglietti, E. V. (1998). The zeta cell: a new ganglion cell type in cat retina. The Journal of Comparative Neurology *399*.

51. Xu, Y., Dhingra, N. K., Smith, R. G., and Sterling, P. (2005). Sluggish and brisk ganglion cells detect contrast with similar sensitivity. Journal of neurophysiology *93*, 2388-2395.

52. Calkins, D. J., and Sterling, P. (2007). Microcircuitry for two types of achromatic ganglion cell in primate fovea. Journal of Neuroscience *27*, 2646.

53. Vardi, N., and Sterling, P. (1994). Subcellular localization of GABAA receptor on bipolar cells in macaque and human retina. Vision Research *34*, 1235-1246.

54. Billups, D., and Attwell, D. (2002). Control of intracellular chloride concentration and GABA response polarity in rat retinal ON bipolar cells. The Journal of Physiology *545*, 183-198.

55. Varela, C., Rivera, L., Blanco, R., and Villa, P. D. (2005). Depolarizing effect of GABA in horizontal cells of the rabbit retina. Neuroscience research *53*, 257-264.

56. Demb, J. B., Zaghloul, K., Haarsma, L., and Sterling, P. (2001). Bipolar cells contribute to nonlinear spatial summation in the brisk-transient (Y) ganglion cell in mammalian retina. Journal of Neuroscience *21*, 7447.

57. Demb, J. B., Zaghloul, K., and Sterling, P. (2001). Cellular basis for the response to second-order motion cues in Y retinal ganglion cells. Neuron *32*, 711-721.

58. Werblin, F. S. (1972). Lateral interactions at inner plexiform layer of vertebrate retina: antagonistic responses to change. Science *175*, 1008.

59. Passaglia, C. L., Enroth-Cugell, C., and Troy, J. B. (2001). Effects of remote stimulation on the mean firing rate of cat retinal ganglion cells. Journal of Neuroscience *21*, 5794.

60. Demb, J. B., Haarsma, L., Freed, M. A., and Sterling, P. (1999). Functional circuitry of the retinal ganglion cell's nonlinear receptive field. Journal of Neuroscience *19*, 9756.

61. Dacey, D., Packer, O. S., Diller, L., Brainard, D., Peterson, B., and Lee, B. (2000). Center surround receptive field structure of cone bipolar cells in primate retina. Vision Research *40*, 1801-1811.

62. Sur, M., and Sherman, S. M. (1982). Retinogeniculate terminations in cats: morphological differences between X and Y cell axons. Science *218*, 389-391.

63. Enroth-Cugell, C., Robson, J. G., Schweitzer-Tong, D. E., and Watson, A. B. (1983). Spatio-temporal interactions in cat retinal ganglion cells showing linear spatial summation. The Journal of Physiology *341*, 279-307.

64. Zaghloul, K. A., Manookin, M. B., Borghuis, B. G., Boahen, K., and Demb, J. B. (2007). Functional circuitry for peripheral suppression in mammalian Y-type retinal ganglion cells. Journal of neurophysiology *97*, 4327.

65. Mills, S. L., and Massey, S. C. (1992). Morphology of bipolar cells labeled by DAPI in the rabbit retina. The Journal of Comparative Neurology *321*.

66. MacNeil, M. A., Heussy, J. K., Dacheux, R. F., Raviola, E., and Masland, R. H. (2004). The population of bipolar cells in the rabbit retina. The Journal of Comparative Neurology *472*.

67. Molnar, A., and Werblin, F. (2007). Inhibitory feedback shapes bipolar cell responses in the rabbit retina. Journal of Neurophysiology *98*, 3423.

68. Roska, B., and Werblin, F. (2003). Rapid global shifts in natural scenes block spiking in specific ganglion cell types. Nature neuroscience *6*, 600-608.

69. Shannon, C. E., and Weaver, W. A mathematical theory of communication, 1948. Bell Syst. Tech. J *27*, 623.

70. Gummer, A. W. (1991). First order temporal properties of spontaneous and tone-evoked activity of auditory afferent neurones in the cochlear ganglion of the pigeon. Hearing research *55*, 143–166.

71. Tiesinga, P. H. E., Fellous, J. M., Jos, J. V., and Sejnowski, T. J. (2002). Information transfer in entrained cortical neurons. Network: Computation in Neural Systems *13*, 41–66.

72. Vaculin, S., Franek, M., Andrey, L., Rokyta, R., Potentials, A., Nuclei, I. T., and Models, N. (2004). Paradoxical firing of thalamic neurons under neuropathic pain state in rats. Neuroendocrinology Letters *25*, 407–410.

73. Zheng, X., Tian, X., Liu, T., and Tao, H. (2008). Entropy Coding of Neuron Firings at Hippocampus CA1 for Memory Dysfunctional Mice. In Natural Computation, 2008. ICNC'08. Fourth International Conference on.

74. Cohen, J. (1988). Statistical power analysis for the behavioral sciences, Hillsdale, NJ: L, (Erlbaum Associates).

75. Rodieck, R. W. (1965). Quantitative analysis of cat retinal ganglion cell response to visual stimuli. Vision Res *5*, 583-601.

76. Enroth-Cugell, C., and Robson, J. G. (1966). The contrast sensitivity of retinal ganglion cells of the cat. The Journal of Physiology *187*, 517.

77. Lukasiewicz, P. D., and Shields, C. R. (1998). Different combinations of GABA A and GABA C receptors confer distinct temporal properties to retinal synaptic responses. Journal of neurophysiology *79*, 3157-3167.

78. Eggers, E. D., and Lukasiewicz, P. D. (2006). Receptor and transmitter release properties set the time course of retinal inhibition. Journal of Neuroscience *26*, 9413.

79. Eggers, E. D., McCall, M. A., and Lukasiewicz, P. D. (2007). Presynaptic inhibition differentially shapes transmission in distinct circuits in the mouse retina. The Journal of Physiology *582*, 569.

80. Palmer, M. J. (2006). Functional segregation of synaptic GABAA and GABAC receptors in goldfish bipolar cell terminals. The Journal of Physiology *577*, 45.

81. Kim, K. J., and Rieke, F. (2001). Temporal contrast adaptation in the input and output signals of salamander retinal ganglion cells. Journal of Neuroscience *21*, 287.

82. Rieke, F. (2001). Temporal contrast adaptation in salamander bipolar cells. Journal of Neuroscience *21*, 9445.

83. Baccus, S. A., and Meister, M. (2002). Fast and slow contrast adaptation in retinal circuitry. Neuron *36*, 909–919.

84. Thoreson, W. B., and Burkhardt, D. A. (2003). Contrast encoding in retinal bipolar cells: current vs. voltage. Vis. Neurosci *20*, 19-28.

85. Shen, W., and Slaughter, M. M. (1998). Metabotropic and ionotropic glutamate receptors regulate calcium channel currents in salamander retinal ganglion cells. J. Physiol. (Lond.) *510 (Pt 3)*, 815-828.

86. Robbins, J., Reynolds, A. M., Treseder, S., and Davies, R. (2003). Enhancement of low-voltage-activated calcium currents by group II metabotropic glutamate receptors in rat retinal ganglion cells. Mol. Cell. Neurosci *23*, 341-350.

87. Yu, J., Daniels, B. A., and Baldridge, W. H. (2009). Slow excitation of cultured rat retinal ganglion cells by activating group I metabotropic glutamate receptors. J. Neurophysiol. Available at: http://www.ncbi.nlm.nih.gov/pubmed/19846623 [Accessed October 26, 2009].

88. Koch, K., McLean, J., Berry, M., Sterling, P., Balasubramanian, V., and Freed, M. A. (2004). Efficiency of information transmission by retinal ganglion cells. Current Biology *14*, 1523-1530.

89. Jaeger, D. (2007). Pauses as Neural Code in the Cerebellum. Neuron *54*, 9-10.

90. Steuber, V., Mittmann, W., Hoebeek, F. E., Silver, R. A., De Zeeuw, C. I., Häusser, M., and De Schutter, E. (2007). Cerebellar LTD and pattern recognition by Purkinje cells. Neuron *54*, 121-136.

91. Wang, P., and Slaughter, M. M. (2005). Effects of GABA receptor antagonists on retinal glycine receptors and on homomeric glycine receptor alpha subunits. Journal of neurophysiology *93*, 3120-3126.

FIGURES

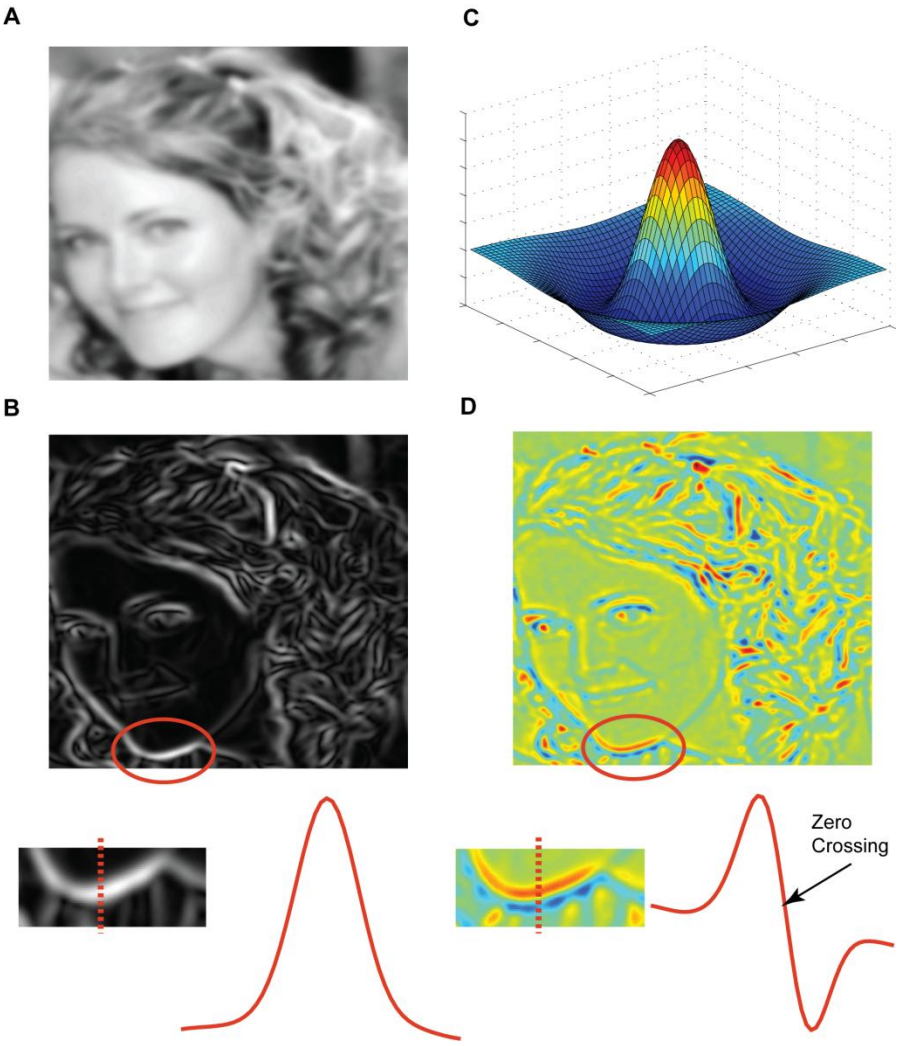

Figure 1. Edge Detection Algorithms.
(A) Original picture used in algorithms in parts (B) and (D).
(B) Image in (A) with a Sobel filter applied. Select area (circled, insert) with an intensity plot of the dotted area is shown below.
(C) Example difference-of-Gaussian (Laplacian) function used to obtain (D).
(D) Laplacian function (C) applied to image (A). Select area (circled, insert) with an intensity plot of the dotted area is shown below.

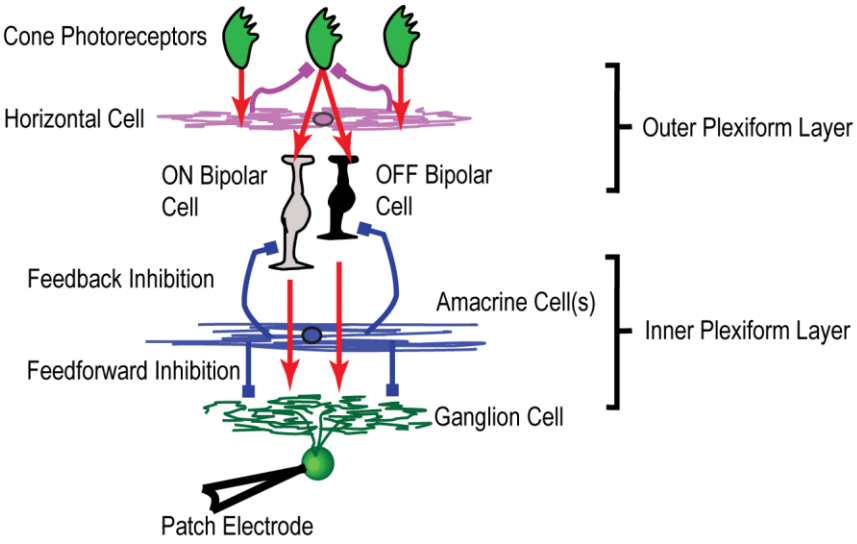

Figure 2. General Retinal Circuitry.
Cones respond to increments and decrements in light with increase or decrease in glutamate release, respectively. All glutamate synapses are represented with red arrows. Horizontal cells and bipolar cells are driven by glutamate from cones in the outer plexiform layer. Horizontal cells modulate cone glutamate release (pink lines). In the inner plexiform layer, ON and/or OFF bipolar cells drive ganglion cells via glutamate release. Inhibitory amacrine cells use GABA or glycine to inhibit bipolar cell terminals (feedback inhibition) or ganglion cells directly (feedforward inhibition).

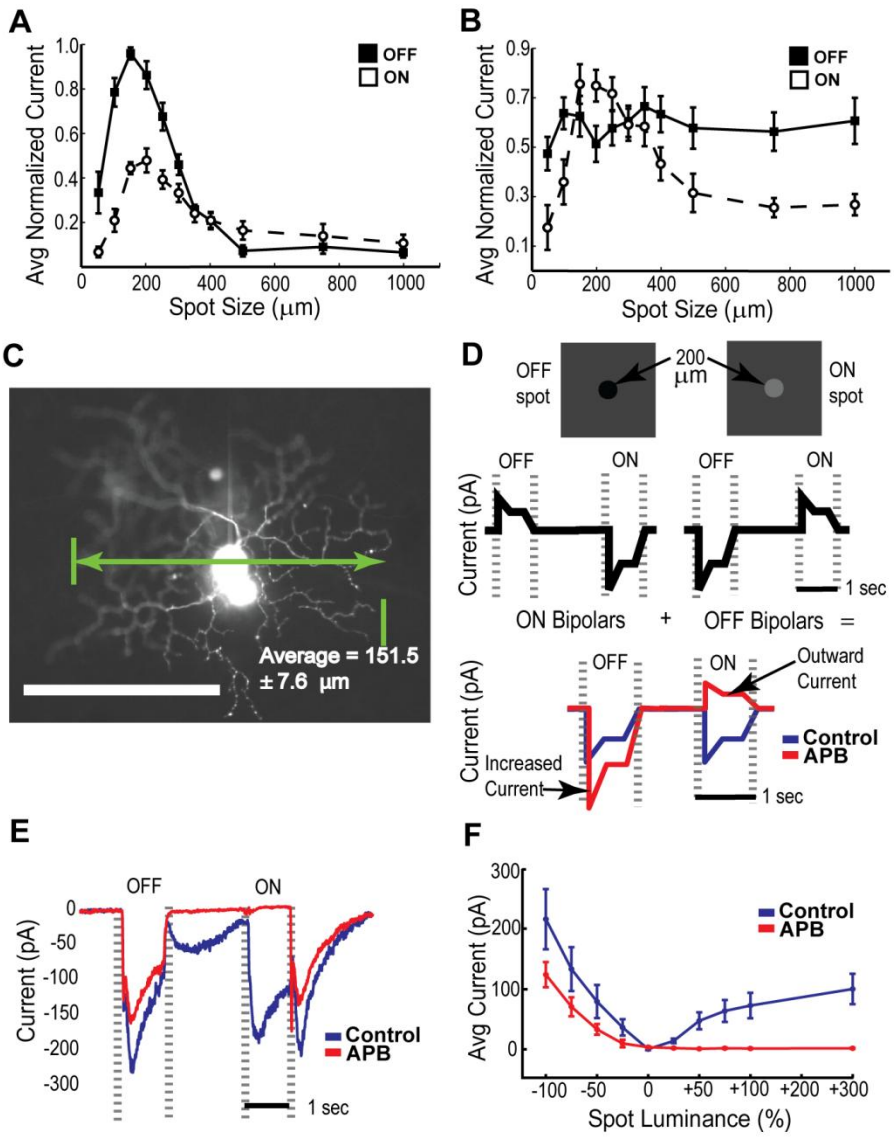

Figure 3. Basic Receptive Field Measurements and Pharmacology for ON and OFF Excitation and Feedforward Inhibition.

(A-B) Average excitatory currents (A) and feedforward inhibitory currents (B) were measured for OFF (-100% luminance) and ON (+300% luminance) spots of varying size and normalized to the maximum measured average current. Error bars = SEM, n=6.

(C) Example of an anatomic photomicrograph of LED filled with Alexa-488 during electrophysiological recording, with average dendritic field size measurement. Scale bar=100 μm, n=13.

(D) Illustration showing summation of nonrectified (linear) ON and OFF excitatory inputs and hypothetical recordings under control and APB in response to 200 μm OFF and ON spots (shown at top). Individual bipolar cell responses (black) are linear; ON bipolar cells respond to OFF spots by reducing glutamate output, and OFF bipolar cells respond to ON spots by reducing glutamate output. The two sets of currents sum together at the LED's dendrites (blue), and APB perfusion (red) reveals outward currents at ON, and an increase in currents at OFF.

(E) Average of responses to OFF and ON spots for control and in the presence of APB, n=9.
(F) Average excitatory current measurements in response to 200 μm OFF and ON spots under control and APB perfusion. Error bars=SEM, n=9.

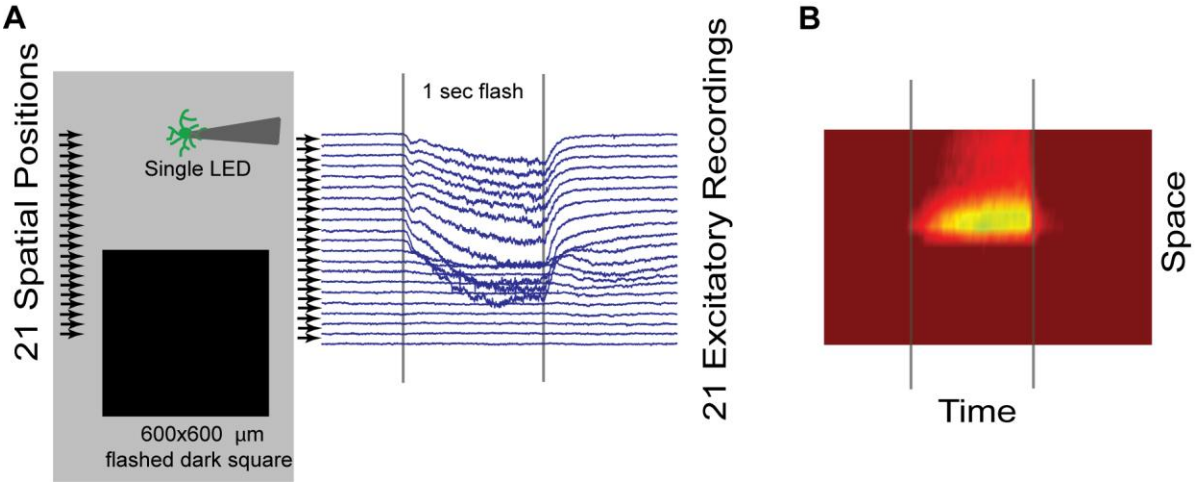

Figure 4. Construction of Spatio-Temporal Edge Rasters.
(A) A single LED is whole-cell patch-clamped and held at -60 mV. A 600 × 600 µm dark square is flashed for 1 sec on grey background at 21 successive spatial positions encompassing the surround and center of the receptive field. A separate recording is taken for each position.
(B) Each recording is lined up in spatial order and plotted as a space-time heat map.

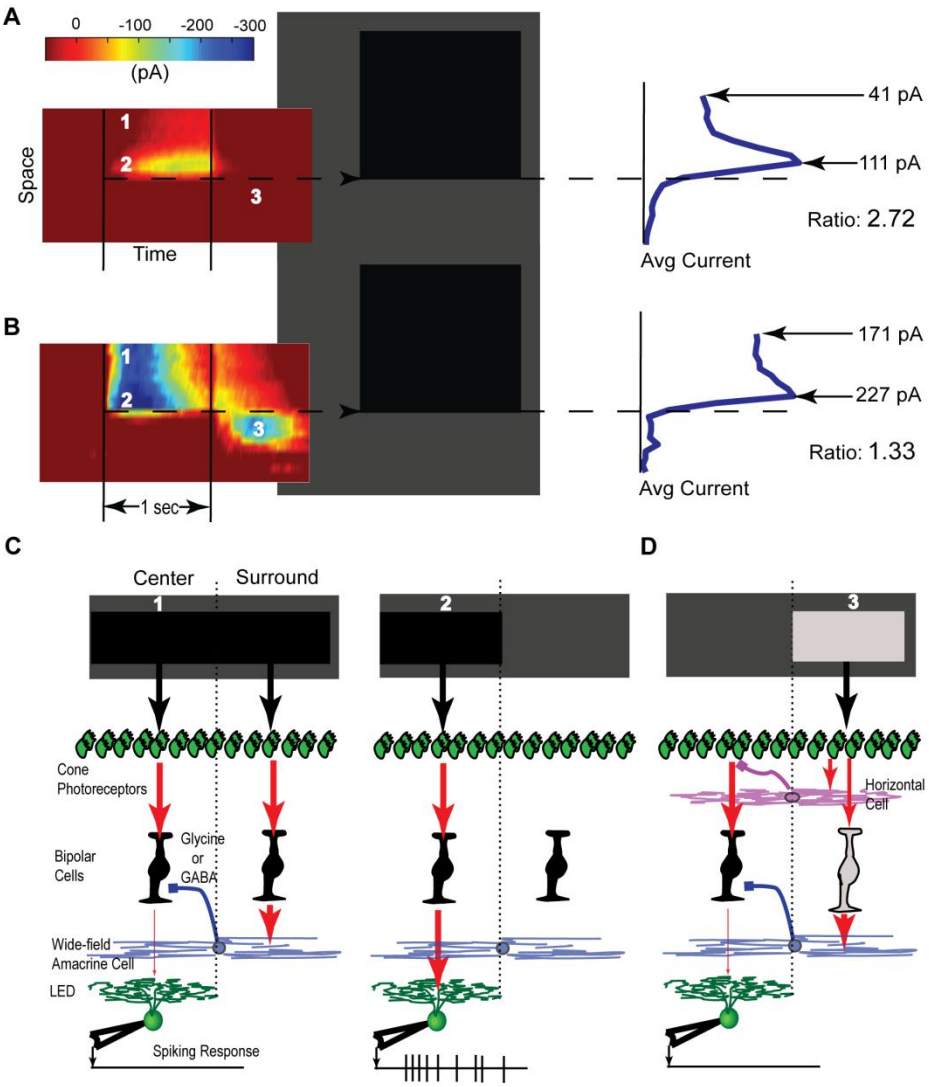

Figure 5. Edge Representation of Feedback Inhibition Under Control and Pharmacologic Blockage.

(A-B). Spatio-temporal raster response to a 600 x 600 µm dark square against a grey background under (A) control conditions or (B) blockage of GABAa, GABAc, and glycinergic systems. The color legend above shows the magnitude of excitatory current (pA). A spatial profile of average currents is to the right, with current magnitude as the x-axis, and spatial location as the y-axis. Measurements of currents for locations distal and proximal to the edge are shown, as well as the ratio of proximal/distal.

(C) Circuit illustration at spatio-temporal locations 1 and 2 (as depicted in (A) and (B) in white numbers). Cells located distally to the edge (location 1) receive more feedback inhibition via wide-field amacrine cells than cells located proximally (location 2), causing larger suppression of excitation.

(D) Circuit illustration at spatio-temporal location 3. The disappearance of the square (indicated as an increase in luminance) causes horizontal cells to increase cone glutamate release in the center, which in turn generates excitation in OFF bipolar cells. This is subsequently suppressed by feedback inhibition induced by this same luminance increment.

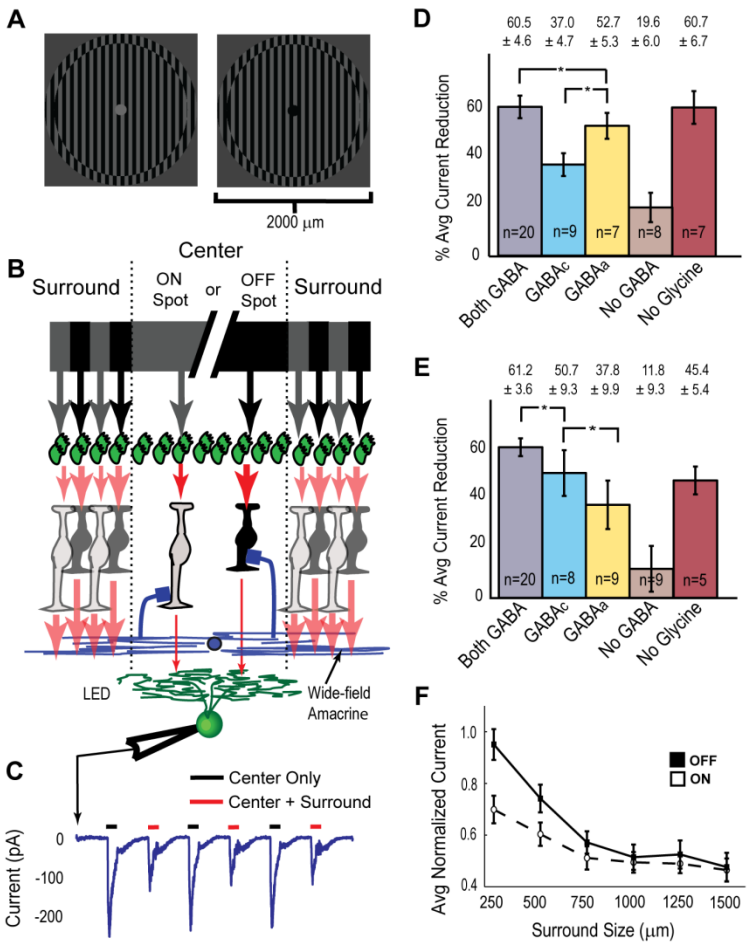

Figure 6. Presynaptic Inhibition by GABAa and GABAc: Reduction in Excitation and Receptive Field Measurements.

(A) Stimuli used in (C-E). The center 150 µm was either solid ON (+300% luminance) or OFF (-100% luminance). All stripes were 50 µm and flipped luminance polarity at 2 Hz.

(B) A circuit diagram of the flow of information through an inner plexiform layer feedback inhibition pathway. Cones release glutamate (red arrows) onto ON or OFF bipolar cells (indicated in grey and black, respectively) in center and surround locations. Center bipolar cells stimulate LEDs by releasing glutamate. Surround bipolar cells release glutamate which drives wide-field amacrine cells, which in turn suppress glutamate release in bipolar cell terminals (blue lines).

(C) An example excitatory current trace (for an OFF center spot) in response to center only (spot) stimulation versus center and surround (grating) stimulation.

(D-E) Average excitatory current reduction of center spot stimulation when full-field flipping gratings are used in the surround for (D) OFF for (E) ON. Bars represent percentage of this reduction under various pharmacologic conditions. Error bars=SEM, n values as indicated for each condition. Values for GABA conditions that are not significantly different are indicated (*).

(F) Average normalized excitatory current of OFF and ON center spot stimulation for increasing areas of flipping gratings in the surround. All currents levels were normalized against a solid 150-µm center spot. Error bars=SEM, n=17 for OFF system, n=20 for ON system.

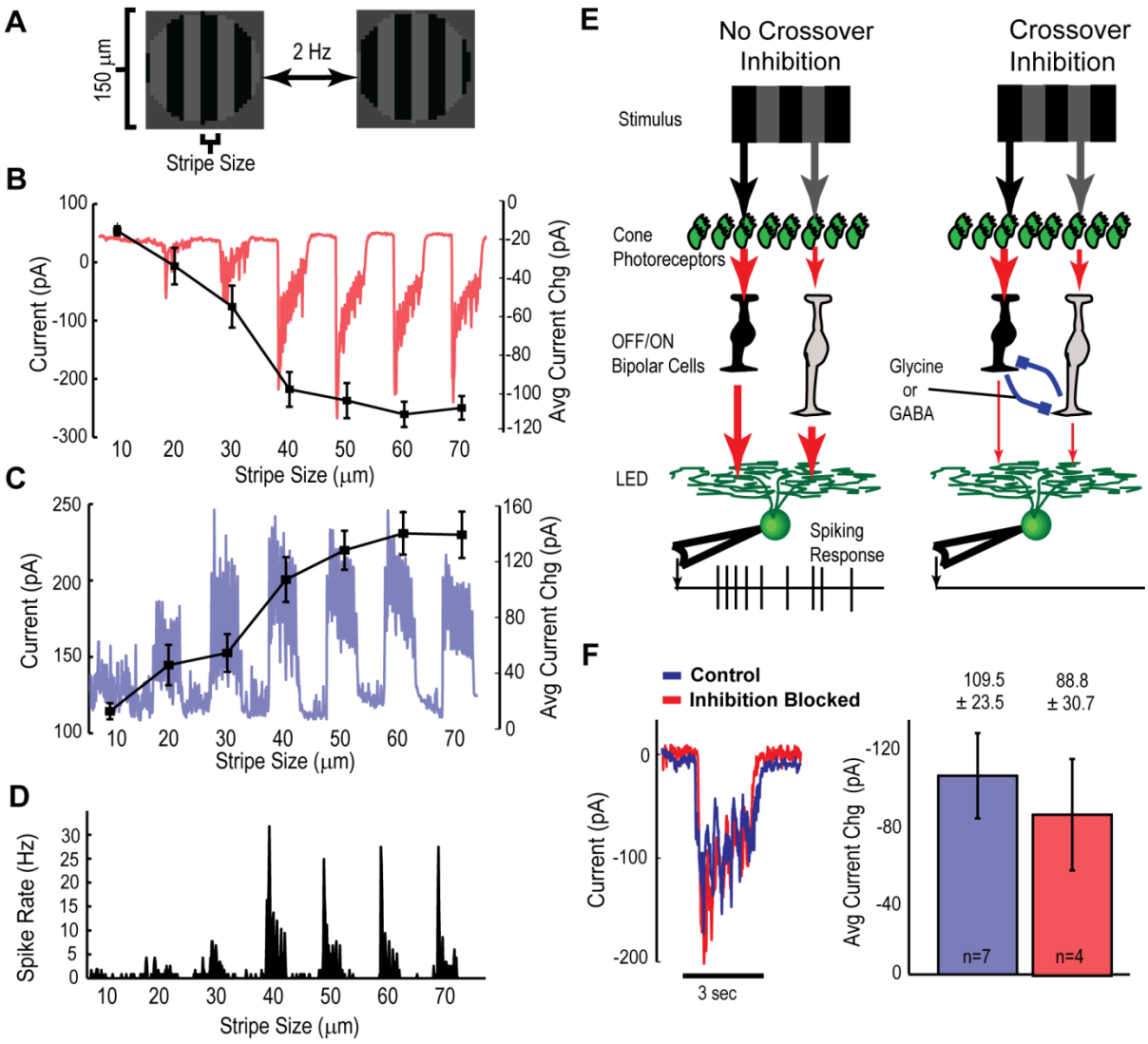

Figure 7. Stimulation of LED-Receptive Field Subunits.
(A) Example of the stimulus presented. The stripe width varied from 10 to 70 µm and was flipped at 2 Hz for 3 seconds. The background was grey.
(B-C) An example excitatory current trace (B) and example inhibitory current trace (C) in response to the series of stimuli described in (A) (red, scale left). Average current change in response to each stripe width (black, scale right). All error bars=SEM, n=10.
(D) Average spike rate in response to stimuli presented in (A), n=8.
(E) A diagram of the circuitry showing the influence of possible crossover inhibition as described in [67]. Red arrows indicate glutamate release, with line weighting indicating relative release levels.
(F) Average currents in response to 50-µm stripes under control and blockage of inhibition (GABAa, GABAc, and glycine). Bar chart indicates average current elicited under control (blue) and inhibition blocked (red). Error bars = SEM.

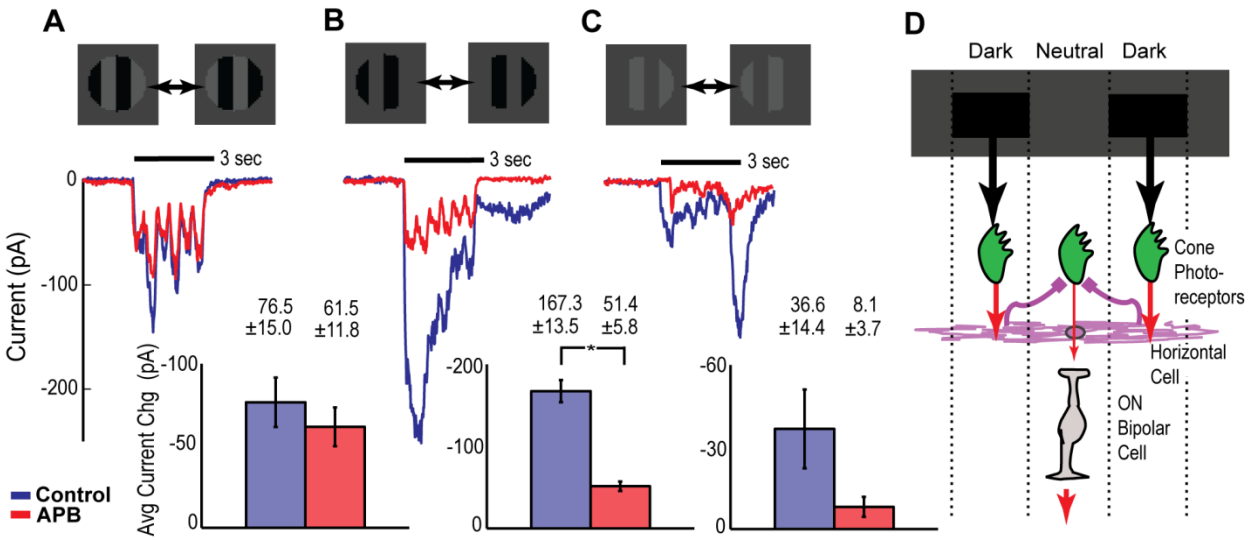

Figure 8. Responsiveness and Contributions of Individual Excitatory Components to Subreceptive-Field Detail.

(A-C) Excitatory recording in response to (A) a luminance-neutral flipping grating with 50-µm stripes, (B) consisting of only dark bars and (C) consisting of only light bars. The first row shows the stimulus. The second row shows average current measurements for control and APB perfusion. Error bars = SEM, n=5.

(D) An illustration of how stimulation of horizontal cells induces currents in ON bipolar cells bearing mGluR6 receptors. Red arrows indicate glutamate release, with line weighting indicating relative release levels. Pink lines indicate horizontal cell-mediated suppression of glutamate release at cone terminals. The luminance change in the stimulus from (B) causes horizontal cells to suppress glutamate release in cone terminals located underneath the grey (neutral) bars. ON bipolar cells bearing mGluR6 receptors that are cospatial with these cones are excited by this glutamate reduction.

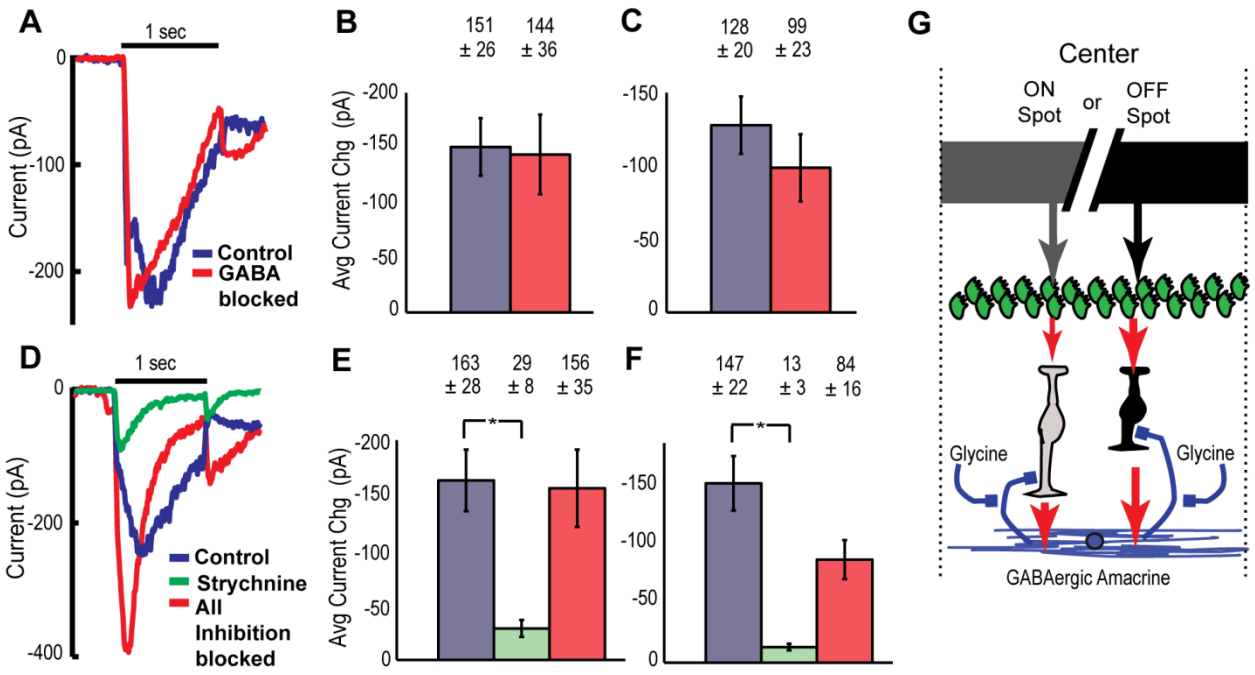

Figure 9. Effect of Pharmacologic Blockage upon Currents Elicited by Spots in the Center.
(A) Average excitatory recordings of an OFF spot (200 µm) under control and GABA blockage, n=8.
(B-C) Average current magnitudes for (B) OFF spots and (C) ON spots under control and GABA blockage. Error bars = SEM, n=8.
(D) Average excitatory recordings of an OFF spot under control, strychnine, and subsequent addition of GABA blockers (all inhibition blocked). Error bars = SEM, n=8 for strychnine, n=6 for all inhibition blocked.
(E-F) Average current magnitudes for OFF spots (E) and for ON spots (F) under control, strychnine, and subsequent addition of GABA blockers (all inhibition blocked). Error bars = SEM, n=8 for strychnine, n=6 for all inhibition blocked.
(G) Illustration of circuit that produces results indicated in (A-F). Red arrows indicate glutamate release. Blue lines indicate inhibitory pathways. Glycinergic inhibition suppresses GABAergic feedback inhibition to bipolar cell terminals, preventing excitatory currents from being inhibited.

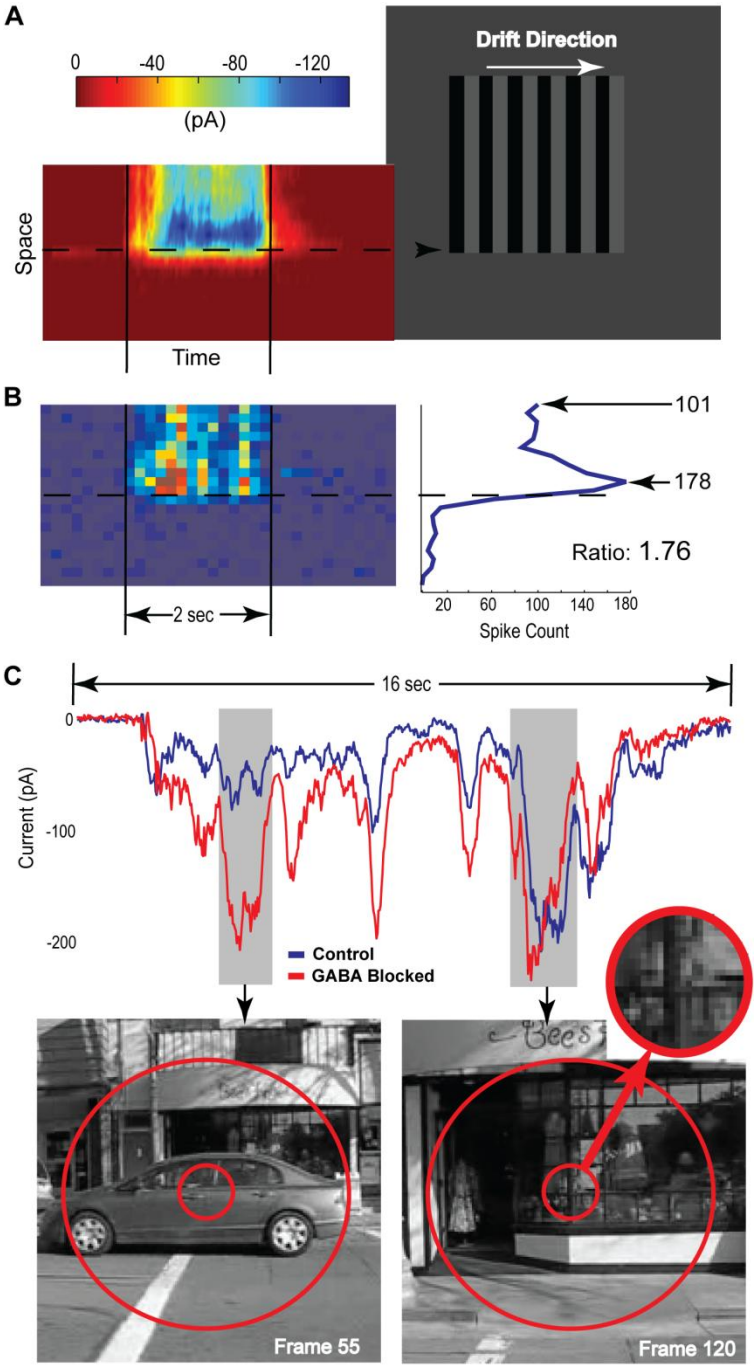

Figure 10. Excitatory Response to Textured Edges and Natural Scenes.
(A) Excitatory spatio-temporal raster plot to a modified raster. The stimulus consisted of a 600 x 600-µm square against a grey background containing luminance-neutral 50-µm stripes, drifted at 2 Hz during the duration of the square's appearance (2 sec). The color legend above shows the magnitude of excitatory current (pA). (B) Binned spiking response to this raster, and summed spike count for each spatial location, n=15. Each bin represents 166 ms in time. A spatial profile of average currents is to the left, with spike count on the x-axis, and spatial location as the y-axis. Measurements of spikes for locations distal and proximal to the edge are shown, as well as the

ratio of proximal/distal.
(C) Excitatory recording in response to a natural scene under control (blue) and GABA blocked (red). Two areas of the recording (grey bars) are selected for closer examination: Frames corresponding to the peaks of excitation under GABA blockage are shown. Concentric circles corresponding to the center (150 μm) and surround (750 μm) are overlayed in red. For the right frame, a blow-up of the image within the center circle is inserted.

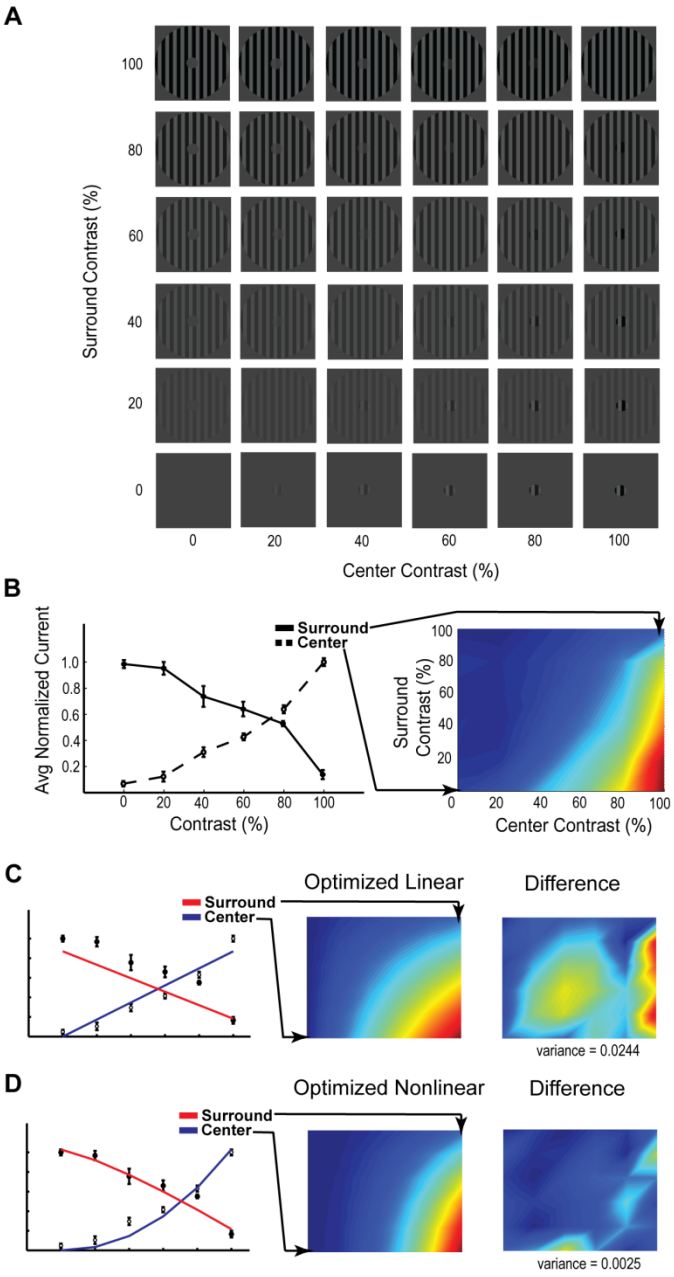

Figure 11. Excitatory Response to Center-Surround Combinations, Optimized Models.
(A) Stimuli used to generate heat plot depicted in (B). Six center contrast and six surround contrast levels were presented and flipped at 2 Hz for a total of 36 stimuli.
(B) Average normalized excitatory currents were assembled into a heat plot (right). Graph (left) depicts currents at fixed center contrasts (solid line) and fixed surround contrasts (dashed line). Error bars = SEM, n = 6.
(C-D) Values from the heat plot in (B) were fitted to a linear (C) or nonlinear (D) center-surround interaction model and subtracted from the original heat plot to obtain the error plot (right). The plot depicts the model values (red and blue) against the recorded excitatory values depicted in the plot in (B).

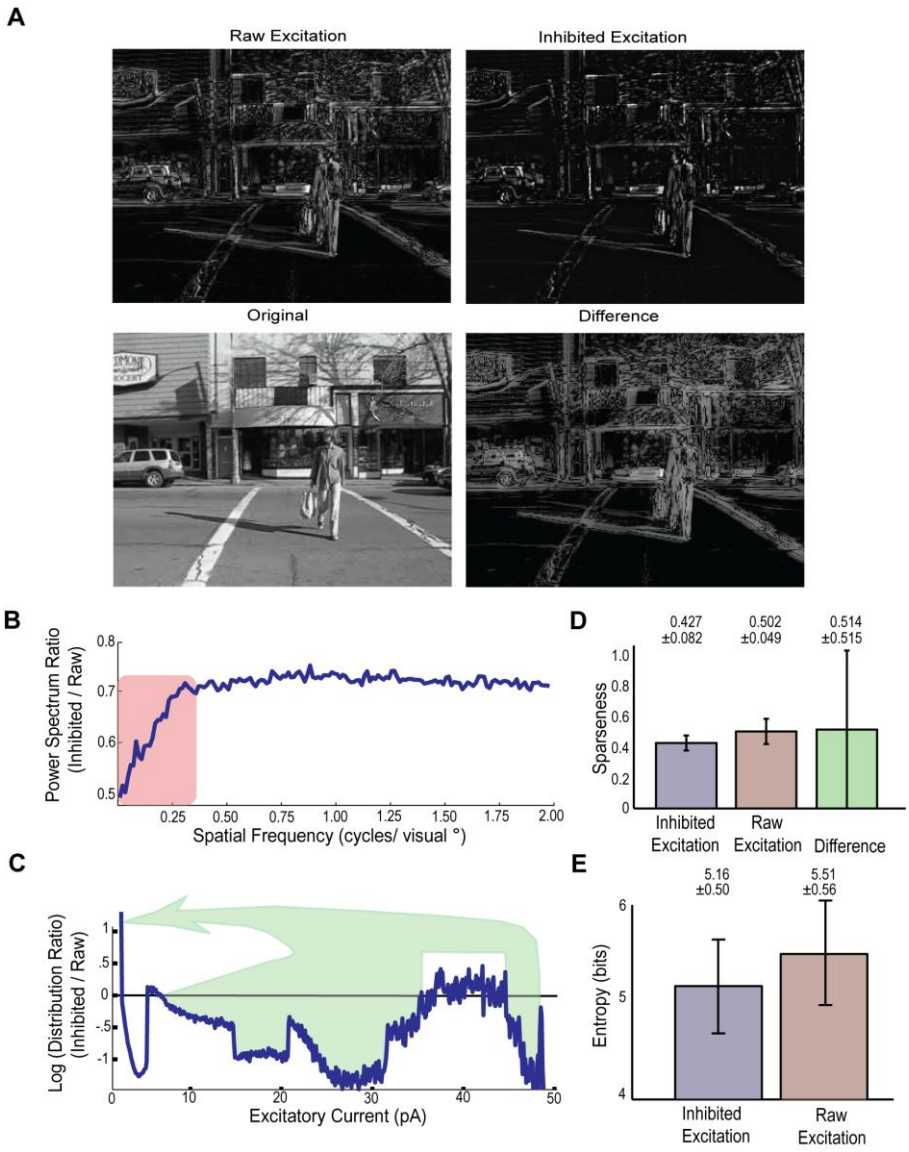

Figure 12. Effect of Feedback Inhibition Upon Scene Statistics.
(A) Original scene (lower left) was modeled by simulated LED excitation with no feedback inhibition ('raw', upper left), with feedback inhibition (upper right), and the difference between both feedback simulations (lower right).
(B) Log of the ratio of power spectra obtained for spatial frequencies present in inhibited versus raw models.
(C) Log of the ratio of simulated currents present at every point in space for inhibited versus raw models.
(D) Measure of sparseness for raw, and inhibited models, plus for their difference. Error bars = standard deviation, n = 30 frames.
(E) Measure of entropy for inhibited and raw models. Error bars = standard deviation, n = 30 frames.

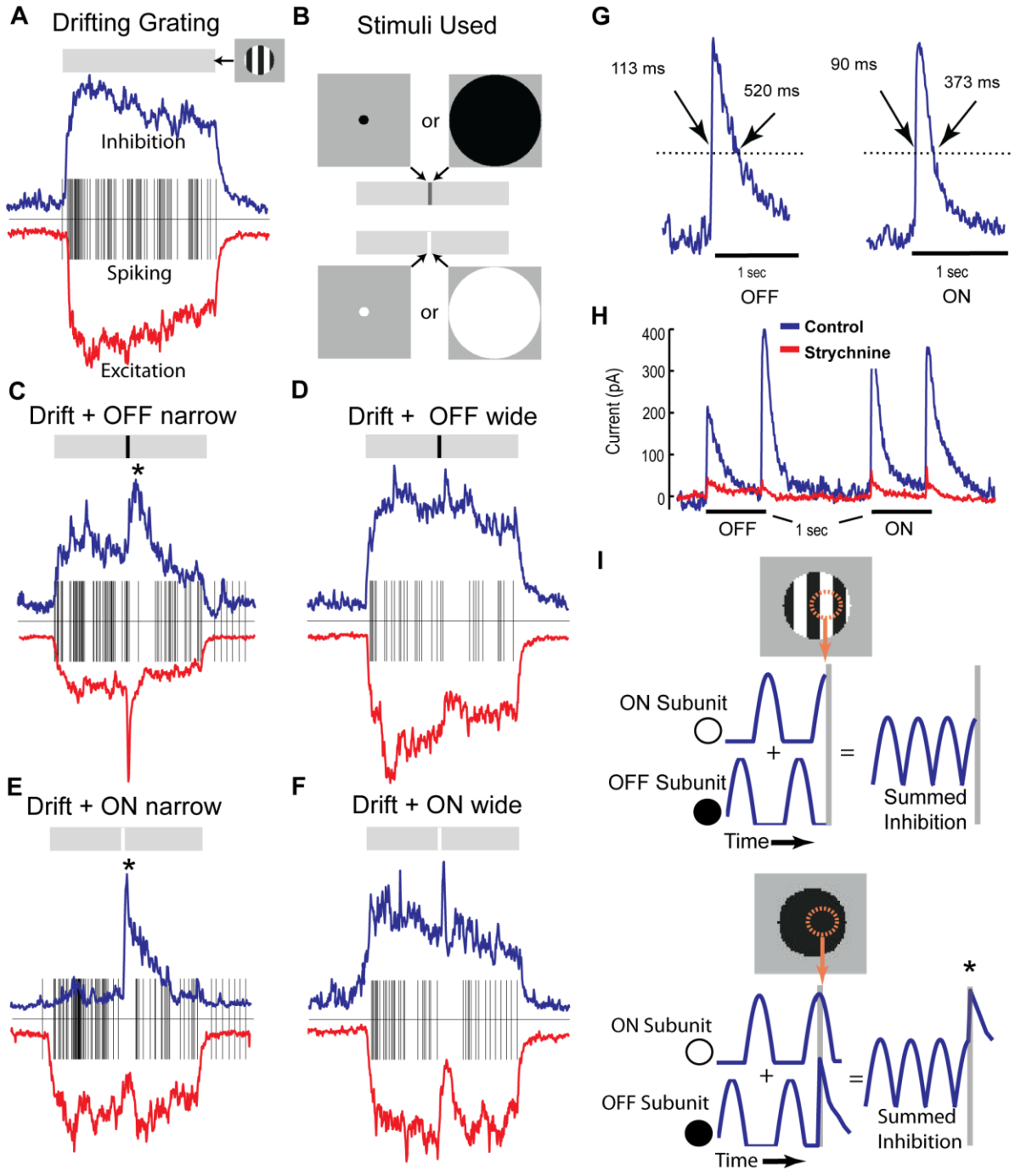

Figure 13. Interaction of excitation and feedforward inhibition during rapid luminance shifts.

(A) Excitation (red), feedforward inhibition (blue), and spiking (black), in response to a drifting grating in the center 150 μm of the receptive field (duration of the drift is indicated with grey bar).

(B) Description of the stimuli used for (C-F). Drifting grating is presented for the duration of the

grey bar. One of the four indicated images is presented for 133 ms at the time represented by the dark (OFF stimuli) or white (ON stimuli) bar.
(C-F) Response to a drifting grating with an OFF (-100% luminance) narrow (150-μm) flash (C), an OFF wide (1000-μm) flash (D), an ON (+100% luminance) narrow flash (E), and an ON wide flash (F).
(G) Rise and decay half-maximum times for OFF and ON feedforward inhibition in response to an OFF (-100% luminance) or ON (+100% luminance) spot, n = 5.
(H) Pharmacology of feedforward inhibition. OFF (-100% luminance) and ON (+100% luminance) spot recordings under control (blue) and 1 μM strychnine perfusion (red), n = 5.
(I) Illustration of response of feedforward inhibition during a drifting grating and luminance shift to dark. Top panel: ON and OFF subunits (located in orange circle) have counter-phasic responses during a drifting grating (blue traces) and sum to produce inhibitory input. Bottom panel: Upon a shift to dark luminance, OFF subunits become activated, adding to already active ON subunits, producing a wave of inhibition on top of the baseline (*), corresponding to the peaks seen in (C) and (D).

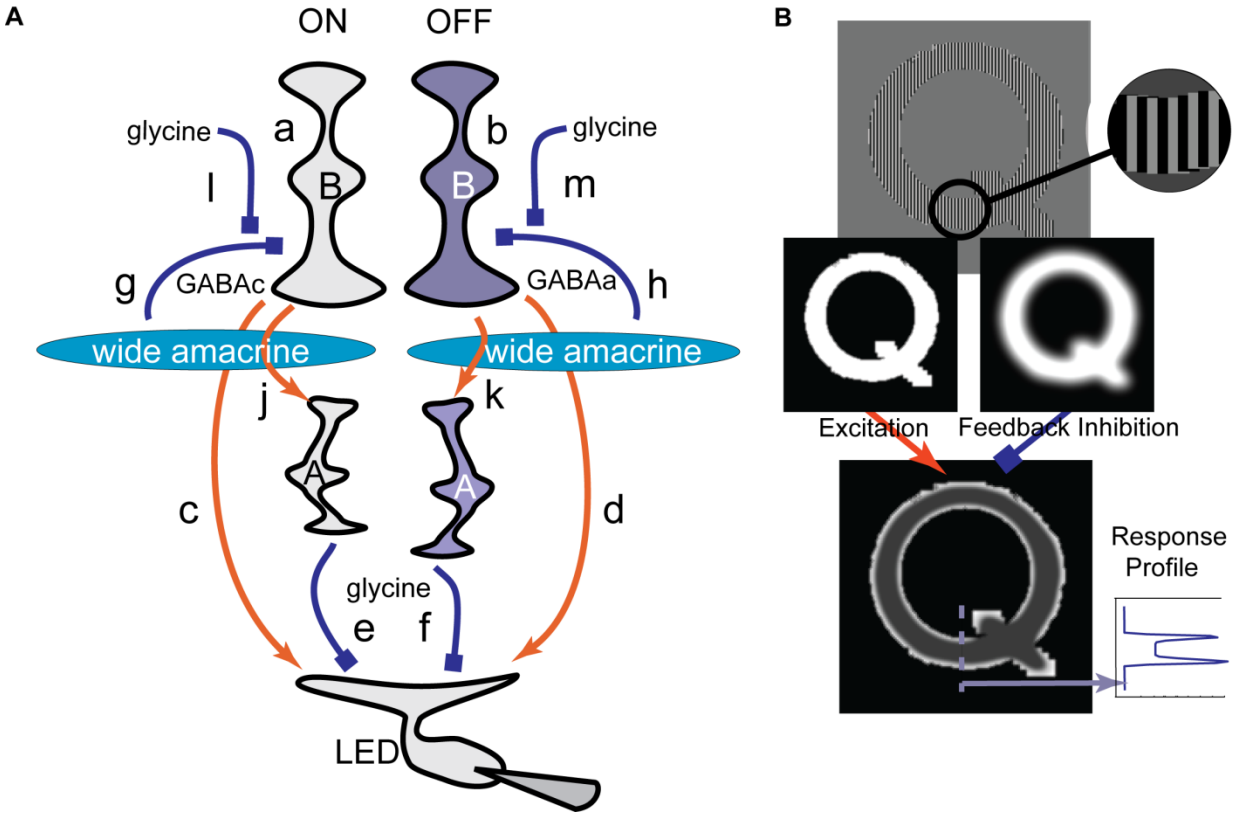

Figure 14. Local Edge Detector Circuit Summary and Illustration of Textured Edge Detection Mechanism.

(A) Illustration of the pharmacologic pathways mediating LED activity. (a, b): ON and OFF bipolar cells. (c, d): ON and OFF rectified high resolution excitatory pathways to LED dendrites. (e, f): high resolution ON and OFF glycinergic feedforward pathways. (g, h): high resolution, wide-field GABAa and GABAc feedback pathways to ON and OFF bipolar cells. (j, k): high resolution excitatory ON and OFF inputs to ON and OFF glycinergic narrow field amacrine cells. (l, m): Center-restricted glycinergic suppression of GABA feedback.

(B) Illustration of Textured Edge Detection Mechanism. Excitation is represented sharply due to the small 150-µm excitatory receptive field of the LED. Feedback inhibition is more blurry due to its larger 750-µm receptive field. Both respond to bipolar-sized detail, and the difference between excitation and inhibition generates a strong response at the edge of the textured area.